



**CHALMERS**  
UNIVERSITY OF TECHNOLOGY

---



# **3D Modelling of Facial Skin Surface for 3D Printing**

Master's thesis in Biomedical Engineering

Emma Ekberg



MASTER'S THESIS 2017:EX056

# 3D Modelling of Facial Skin Surfaces for 3D Printing

EMMA EKBERG



Department of Electrical Engineering  
*Division of Signal Processing and Biomedical Engineering*  
CHALMERS UNIVERSITY OF TECHNOLOGY  
Gothenburg, Sweden 2017

3D Modelling of Facial Skin Surfaces for 3D Printing  
EMMA EKBERG

© EMMA EKBERG, 2017.

Supervisor: Paul Gateholm, 3D Bioprinting Center, Department of Chemistry and Chemical Engineering, Chalmers University of Technology  
Examiner: Fredrik Kahl, Department of Electrical Engineering, Chalmers University of Technology

Master's Thesis 2017:EX056  
Department of Electrical Engineering  
Division of Signal Processing and Biomedical Engineering  
Chalmers University of Technology  
SE-412 96 Gothenburg  
Telephone +46 31 772 1000

Cover: Point cloud of a face reconstructed using images from a digital camera.

Typeset in L<sup>A</sup>T<sub>E</sub>X  
Printed by [Name of printing company]  
Gothenburg, Sweden 2017

## Abstract

One of the major global health problems today is burns, with an estimate of 256 000 deaths each year caused by fires [1]. For more severe burns the probability of infections increases and here the golden standard is to use autologous skin grafts. However, the dressing covering the skin grafts has a problem the taking of the graft when it comes to convex surfaces. The solution is to create a patient specific dressing that conforms to the surface by creating a 3D model of the wounded area of the patient, which then can be 3D printed.

The aim of this project is to analyze the process of converting images of facial skin surfaces into a 3D model using both active and passive scanning techniques. The project also analyses what is required for the model to be 3D printed, with the aim of a patient specific dressing.

The different scanning techniques that have been used are: a digital camera, an advanced image based 3D camera and a 3D scanner. The model obtained from the 3D scanner was used as a ground truth. The acquired data was then reconstructed into a 3D model using available softwares. The model was also 3D printed using different kinds of printers with two kinds of materials: plastic and hydrogel.

The advanced 3D camera gave accurate models which was suitable for imaging patients that moves. The imaged based method using a digital camera can, under right conditions, be a sufficient method for 3D modelling smooth, convex surfaces. It was also possible to 3D print a convex surface using both plastic and hydrogel, where the shape was maintained overall except for some collapsing when printing with the hydrogel.

The project shows that a patient specific dressing may be a possibility in the future. However, the problem is not to obtain a accurate 3D model of the patient, but to maintain this accuracy when 3D printing with different materials. In the future, the ideal scenario is to 3D scan a patient and then directly 3D print a dressign, which will fulfill the entire need of the wound of the patient.

Keywords: 3D printing, 3D bioprinting, 3D modelling, patient specific bandage.



# Acknowledgements

This project would not have been possible without the support and expertise of other individuals and organizations. Firstly I would like to thank my supervisor, Paul Gatenholm, for the unyielding feedback, and my examiner, Fredrik Kahl, for patiently answering all my questions.

Secondly I would like to give a big thanks to my colleague, Caroline Damgaard, for the help with 3D printing with nanocellulose. I would also like to thank Erik Mårtensson Djäken at Innovationsplattformen for the possibility to learn more about the medical procedures at Sahlgrenska University Hospital.

Finally, I have to express my appreciation to Ignasi Fernandez Perez at the Division of Structural Engineering for letting me borrow the HandyScan3D, and the plastic surgeon Lars Kölby at Sahlgrenska Hospital for helping me use the 3dMD scanner. And at last, I am grateful for all the colleagues at the 3D Bioprinting Center Chalmers for following and supporting me through this project.

Emma Ekberg, Gothenburg, June 2017





# Contents

<b>List of Figures</b>	<b>xi</b>
<b>List of Tables</b>	<b>xv</b>
<b>1 Introduction</b>	<b>1</b>
<b>2 Theory</b>	<b>3</b>
2.1 Skin Grafts . . . . .	3
2.1.1 Skin Fixation and Dressings . . . . .	4
2.2 3D Modelling . . . . .	6
2.2.1 Passive Image Based Methods . . . . .	6
2.2.1.1 Structure-from-Motion . . . . .	7
2.2.1.2 Multi View Stereo Algorithms . . . . .	8
2.2.2 Active Scanning Methods . . . . .	8
2.2.3 3D Reconstruction . . . . .	8
2.2.3.1 Poisson Surface Reconstruction . . . . .	9
2.2.3.2 Poisson Disk Sampling . . . . .	11
2.3 Post Processing a Model . . . . .	12
2.3.1 Smoothing of Surface . . . . .	12
2.3.2 Simplification of Surface . . . . .	13
2.3.3 Subdivision of Surface . . . . .	14
2.4 Comparing Models . . . . .	14
2.4.1 Hausdorff Distance . . . . .	14
2.5 3D Printing . . . . .	15
2.5.1 3D Bioprinting . . . . .	17
<b>3 Methods</b>	<b>19</b>
3.1 Data Acquisition . . . . .	19
3.1.1 Digital Camera . . . . .	19
3.1.1.1 Image Acquisition . . . . .	19
3.1.2 Advanced 3D Camera . . . . .	20
3.1.3 3D Scanner . . . . .	20
3.2 3D Modelling . . . . .	21
3.2.1 Dense Point Cloud . . . . .	21
3.2.2 Surface Reconstruction . . . . .	22
3.3 Comparing Models . . . . .	23
3.4 3D Printing . . . . .	23

3.4.1	CAD Design . . . . .	23
3.4.2	3D Printer . . . . .	23
3.4.3	3D Bioprinter . . . . .	24
3.4.3.1	Printability Analysis . . . . .	24
<b>4</b>	<b>Results</b>	<b>27</b>
4.1	3D Modelling . . . . .	27
4.1.1	Digital Camera . . . . .	27
4.1.1.1	Processing Comparison . . . . .	29
4.1.2	Method Comparison . . . . .	34
4.2	3D Printing . . . . .	36
<b>5</b>	<b>Discussion</b>	<b>41</b>
<b>6</b>	<b>Conclusion</b>	<b>43</b>
	<b>Bibliography</b>	<b>45</b>

# List of Figures

2.1	Overview of the process from a patient, where the wounded area is imaged, to 3D printing the 3D model. . . . .	3
2.2	Figure of the bolster adjusted to the shape of the eye, and how the bolster fills up the wound [10]. . . . .	4
2.3	Figure of the bandaging procedure at Sahlgrenska University Hospital, where the wound is covered with a wet protective dressing (tulle gras), filled with a bolster and then wrapped with a gauze bandage. . . . .	5
2.4	Figure of the bandaging procedure using negative pressure at Sahlgrenska University Hospital, where the black dots symbolizes the staples attaching the edge of the skin graft. . . . .	5
2.5	Illustration of how triangulation works. . . . .	7
2.6	Illustrative image of how the Poisson Reconstruction processes an outward oriented point cloud to a surface, using an indicator function and an indicator gradient. . . . .	10
2.7	<i>Image of two iterations of a octree where a voxel subdivides into octants, thus increasing the resolution of the voxel. Each square is a n octree node.</i> . . . .	11
2.8	Poisson Disk Sampling visualised on a bunny, where the distance between samples are viewed in a colour gradient [25]. . . . .	11
2.9	Laplacian smoothing, where a point is repositioned as the average of the adjacent points [26]. . . . .	12
2.10	Two versions of edge collapse. <b>a)</b> Edge collapse by removing two vertices and replacing it with a new. <b>b)</b> Edge collapse by removing one vertex and re-triangulate. . . . .	13
2.11	Illustration of the iterative process of LS3, by first triangulate each polygon, relax the mesh and then project it using least-square (seen as green) [28]. . . . .	14
2.12	The signed distance of the Hausdorff distance, where $d_1$ is positive and $d_2$ is negative, assuming that the surfaces $S_1$ and $S_2$ has normals upwards. . . . .	15
2.13	Overview of the steps from a real object to the printed object. . . . .	16
3.1	Illustration of the static-3dMD system, using 9 cameras evenly distributed around the center, capable of imaging 360 degrees of the upper body. . . . .	21

3.2	The Inkredible 3D bioprinter and the 3D printer MakerBot Replicator 2. . . . .	24
4.1	Version 2 where adhesive patches has been added to create distinct points on the surface of the model. . . . .	28
4.2	To the left is the sparse point cloud and to the right is the dense point cloud obtained of Version 1 using a SfM algorithm and then a MVS algorithm. . . . .	28
4.3	The process from image, to a point cloud and then a reconstructed mesh, with and without color. Bigger holes are circled in red. . . . .	29
4.4	From left to right, version 1-4 reconstructed using default parameters. . . . .	29
4.5	The mesh obtained using HS3D to the left, and the point cloud from Version 1 aligned to this mesh. . . . .	30
4.6	The point cloud from Version 1 and Version 2, to the left and right respectively, compared to the mesh obtained using HS3D. The models has a color scale indicating the distance from the point cloud to the reference model. . . . .	30
4.7	The point cloud of the face of Version 2 compared to the point cloud obtained using HS3D. To the left is a nearest neighbour comparison while to the left is a local comparison. . . . .	31
4.8	The mesh from Version 1 with parameters of Set 1, to the left, and Version 1 with Set 1 that has been smoothed, to the right. The meshes have been compared to the mesh obtained using HS3D. The models has a color scale indicating the distance from the point cloud to the reference model. . . . .	32
4.9	The mesh from Version 1 with Set 4 to the left, and Version 1 with a smoothed Set 1 to the right. The meshes has been compared to the mesh obtained using HS3D. The models has a color scale indicating the distance from the point cloud to the reference model. . . . .	32
4.10	The point cloud from Version 1 to the left, and the sampled point cloud of Version 1 to the right. The point clouds has been compared to the mesh obtained using HS3D. The clouds has a color scale indicating the distance from the point cloud to the reference model. . . . .	33
4.11	The mesh from the smoothed Version 1 with Set 1, to the left, and its mesh from the sampled point cloud with Set 1, to the right. The meshes has been compared to the mesh obtained using HS3D. The models has a color scale indicating the distance from the point cloud to the reference model. . . . .	33
4.12	The process for the 3dMD camera at Sahlgrenska, showing the angles of images of the mannequin, the patterned flash and the resulting mesh. . . . .	34
4.13	From left to right: the mesh form the 3dMD camera, the mesh from the HS3D scanner and the comparison between them. . . . .	35
4.14	Comparing the 3dMD method and the digital camera to the HS3D. From left to right: the 3dMD mesh, the smoothed Version 1 and Version 1 with a lower reconstruction depth. . . . .	35

---

4.15	CAD model of the face mask in blue, and the solid face in red. . . . .	36
4.16	The sliced mask from the CAD model, with yellow indicating the layers and the green is the support structure. . . . .	36
4.17	Three models printed with PLA. From left to right: the solid face, the face mask without support and the face mask with support. . . .	37
4.18	The solid face printed with 3% CNF at 110 Pa. . . . .	37
4.19	Image during the printing of the face mask. To the left is 3% CNF printed at 110 Pa and to the right is Nivea cream printed at 55 Pa. .	38
4.20	The face mask printed with 3% CNF at 110 Pa with a support structure printed with Nivea cream at 55 Pa. . . . .	38
4.21	The printability analysis for 4% CNF versus the Nivea Cream, visualized as printing speed against the radius. . . . .	39
4.22	From left to right: the face mask printed with 1%, 3% and 4% CNF on a Nivea support. The masks was treated with a calcium chloride bath, freeze dried on the Nivea and freeze dried on a plastic support respectively. . . . .	39
4.23	The face mask directly after printing and the freeze dried structure without Nivea cream. . . . .	40



# List of Tables

3.1	Table of the digital camera used, and the two different lenses. The MP stands for megapixel, the focal range indicates the interval of the focal length and f is the maximum aperture. . . . .	19
3.2	Table over different tests taken under different conditions, with different setups. Version 1: Macro lens with low focal length, Version 2: patches, Version 3: unique background, Version 4: Macro lens with high focal length. . . . .	20
3.3	Table over the values of different parameters used to reconstruct the model. . . . .	22
4.1	Table over different version of acquiring images of the mannequin using different conditions, with different setups. . . . .	27





# 1

## Introduction

Today one of the global health problems is burns, which have an estimate of 256 000 deaths each year caused by fires [1]. Burns are injuries to the skin or other tissues usually caused by heat or radiation [1]. One of the most important problems with treating larger burns is complications such as infections [2]. If the burn is severe enough the wound need help to heal and prevent infections, and the solution can be to use autologous skin grafts. Skin grafts is a piece of skin that is transplanted from a healthy site of the patient to the wounded area to facilitate the regeneration of the burn [3]. The new skin graft is thereafter covered with a dressing to facilitate the healing and the taking of the transplanted skin graft.

However, a problem of these dressings occurs when it comes to irregular and complex areas, such as concave surfaces in the face. Here it is preferable that the design of the dressing conforms to the skin surface to increase the probability of the taking. For these complex surface a solution could be to make the dressing uniquely adapted to the area. One mean to accomplish a patient specific dressing is to create a Three-Dimensional (3D) model of the wounded skin surface, which then can be used to create the dressing for the patient.

The idea is to then use the technique of 3D printing to manufacture the designed dressing. With 3D printing the dressing can either be created from a printed mold or 3D printed directly. 3D printing is a technique that manufactures 3D objects by depositing layers of a certain material from a given model [4]. 3D printing has existed since Charles Hull invented it in the early 1980's [5], but it was not until more recently that a lot of patents regarding printing techniques expired and 3D printing began to expand commercially [6]. There are several applications for 3D printing, where the industrial application is the biggest. However for this project it is the use of 3D printing within customized medical devices that is of interest [4]. Examples of medical devices where 3D printing is used are hip replacements and dental implants.

The technique of 3D printing has also enabled a new field called 3D bioprinting. 3D bioprinting uses 3D printing techniques to deposit cells and biomaterials into structures, where the goal is to create structures that resembles organs or tissues [7]. When it comes to skin grafts, the use of 3D Bioprinting enables 3D printing artificial skin instead of transplanting skin from a healthy site of the patient. This is especially beneficial when it comes to large burns, where there might not be enough healthy skin left of the patient to transplant.

This thesis is a part of a bigger project called *Onskin*, which is a newly started project that considers the use of 3D printing within the application of customised 3D dressings. This project is a collaboration between the different companies and organisations: 3D Bioprinting Center Chalmers, Sahlgrenska, Cellink, Stora Enso, Medibiome and APT AB. The final goal of *Onskin* is to create on skin dressings uniquely made for patients that has undergone a skin transplant as a result of severe wounds, such as severe burns. The end goal is to create patient specific dressings for skin grafts where complex areas makes it harder to apply the dressing.

To create a patient specific dressing the first problem is to create a 3D model of the affected area. A 3D model of an object can be created from either medical images or images acquired from an ordinary camera or a scanner. Medical imaging, such as Computerized Tomography (CT) or Magnetic Resonance Imaging (MRI), are more used for imaging internal parts of the body. However, for external parts such as the skin, medical imaging might be extravagant. Instead, techniques using camera images or scanned images are simpler methods of modelling surfaces such as the skin. Methods of imaging the surface in 3D can be divided into active and passive methods depending on whether they measure the depth to an object directly or indirectly [8], [9].

The aim in this thesis is to acquire and convert images of facial skin surfaces into a 3D model using two different techniques, passive and active 3D reconstruction techniques. The project seeks to investigate what is required for the model to be 3D printed. The purpose is to investigate what is required to use the well known technique of 3D surface reconstruction for 3D printing customized medical devices, with focus on patient specific dressings for skin grafts.

# 2

## Theory

This section chronologically explains the theory concerning the process from treating the wound to 3D printing the reconstructed model, see figure 2.1.

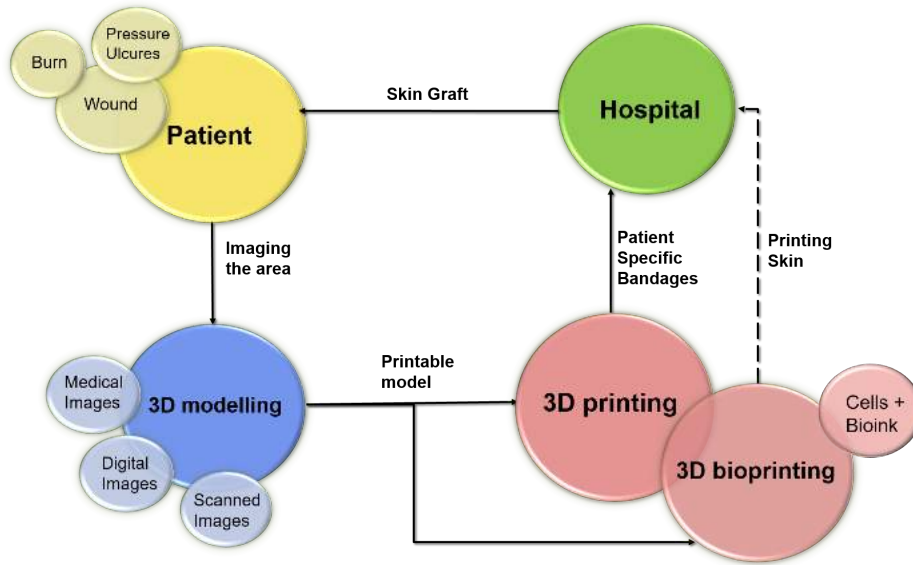


**Figure 2.1:** Overview of the process from a patient, where the wounded area is imaged, to 3D printing the 3D model.

### 2.1 Skin Grafts

The skin is an important organ which has the functions to protect us from the outer environment, regulate temperature and control sensation. Skin is divided into two layers, epidermis and dermis [10]. Epidermis is the top layer which consists of keratinocytes, which are stem cells that gives skin its regenerative capacity and proliferation. Dermis is the bottom layer and consists mainly of connective tissue which gives skin its mechanical properties and contributes to the stability. The main cell type in the dermis layer is fibroblasts, which aids the healing after an injury by activating wound contraction. The dermis also contains the blood vessels and nerve fibres [10].

Skin grafts is often the standard procedure for covering large area of skin loss and severe damages to the skin, such as extensive wounds or burns. The expression *skin*

*graft* can refer to both the actual transplantation and to the transplanted skin. The treatment considers transferring skin from a healthy site of the body to a damaged site. At the damaged site, the skin graft is left intact except for an incomplete blood supply. To decrease the damage from the donor site, the skin graft is usually expanded by creating a meshed skin graft where apertures have been made onto the skin. These holes also allow removal of fluid.

Depending on the conditions, the skin graft is classified into thin split-thickness, thick split-thickness and full-thickness [10]. The difference of the classifications depends on the thickness of the skin graft, that is the amount of epidermis and dermis retrieved.

The healing of the skin graft takes place in different stages. In the first stage the graft will be nourished by liquids, nutrients and oxygen which diffuses between the wound and the graft. The second stage consists of the revascularization, where blood vessels reconnect. This stage is the critical stage and determines the survival of the skin graft. In the last stage, when the graft is fully revascularized, the graft and surrounding tissue matures and starts to contract [10].

Contraction is the process of wound edges moving to the centre of the wound to close it. In humans the skin is firmly attached, in contrary to some animals where the skin is more loose. This can lead to complications in human skin healing where distortions can occur of the surrounding tissue and create infections [10], [11].

### 2.1.1 Skin Fixation and Dressings

In the critical stage of revascularization there are multiple factors that contributes to achieving a stable taking, where an important factor is the immobility of the graft during the revascularization. Therefore the skin graft needs to be fixated to achieve precise contact with the surface of the wound [10]. The conventional procedure is to first suture the skin graft to the wound, thereafter a non-adherent dressing is placed and covered with a gauze or a bolster [12], see figure 2.2 and 2.3. The function of the bolster is to apply a small pressure to precisely adapt the skin graft to the wound and to allow removal of fluid.

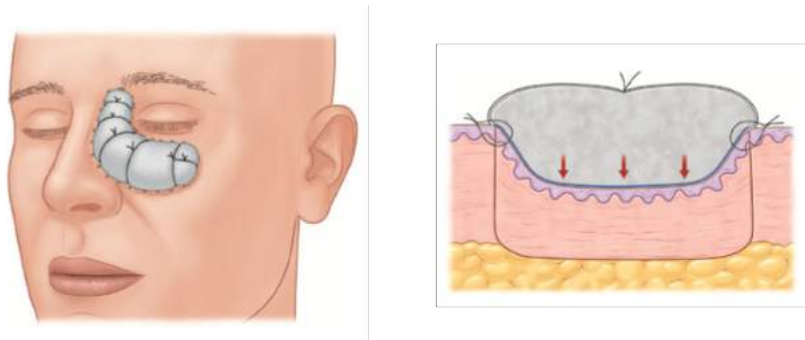


**Figure 2.2:** Figure of the bolster adjusted to the shape of the eye, and how the bolster fills up the wound [10].



**Figure 2.3:** Figure of the bandaging procedure at Sahlgrenska University Hospital, where the wound is covered with a wet protective dressing (tulle gras), filled with a bolster and then wrapped with a gauze bandage.

However, the conventional method of a dressing with a bolster is more suitable for smaller wounds, and here taking of the graft is not always ensured. An additional solution to fixate the graft is to create a negative pressure to the wound and to the graft. Vacuum-Assisted Closure (VAC) dressings is a way of creating negative pressure and is used for larger graft sites or for areas with higher mobility, such as the concave surfaces in the armpit or the lower part of the back [10].

To create a negative pressure a foam sponge is placed to fit precisely into the cavity of the skin graft. Then an adhesive dressing is placed over the sponge to fixate it. A hole in the dressing is made where a tube is placed which creates a suction out from the wound [13]. The suction creates pressure to the entire wound and collects excess fluid. The process can be seen in figure 2.4. It is shown that negative pressure

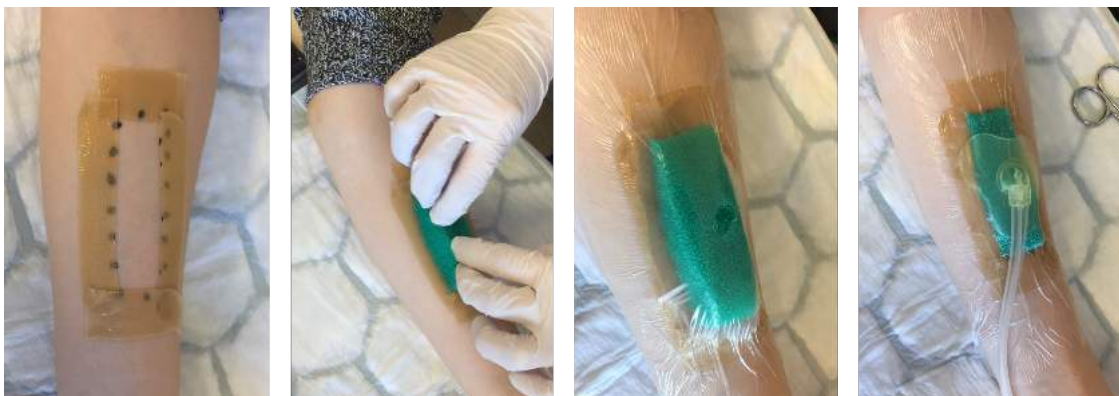


**Figure 2.4:** Figure of the bandaging procedure using negative pressure at Sahlgrenska University Hospital, where the black dots symbolizes the staples attaching the edge of the skin graft.

increases the probability of the taking of the graft [12], [14], where the cause is a combination of factors. The main factors that probably benefit the taking is that negative pressure increases the local blood flow to the wound, immobilizes the graft to maintain the contact to the wound site, and that it removes excess fluid [14].

The use of VAC is a good alternative to the conventional dressing, however there is insufficient evidence of the effectiveness of negative pressure and especially why it benefits wound healing and graft taking [15].

## 2.2 3D Modelling

3D modelling is the general process of 3D reconstructing an object. The most common way of reconstructing a model is to design the object from scratch using Computer-Aided Design (CAD). However, when trying to reconstruct a duplicate of a real object using CAD the process can be time consuming and require some effort [16]. One solution to this is to use various techniques to obtain a 3D model directly from the real object. The main idea is to find out the structure of an object by in different ways obtaining its 3D points and create a surface from this.

Generally there are two types of methods used to obtain a 3D model from a real object, namely using either a passive or an active method. The difference between a passive and active method is that a passive method measures the 3D points from the emitted light from the object, while a active method emits light and then measure the distance to the object directly. Passive methods need further processing of the data to reconstruct 3D coordinates, whilst active methods provides the 3D coordinates directly in the form of a depth map [8], [9].

### 2.2.1 Passive Image Based Methods

Passive methods measures the emitted visible light from the object and they are generally image based methods that acquire 3D reconstruction from multiple views [8], [9]. Imaged based 3D reconstruction can be described as algorithms that estimates the 3D model of an object based on stereo vision with set of images taken with a camera [17].

The idea is to mimic the image reconstruction of the human vision, which can sense depth and distance of an object from a 2D vision. Since we have two eyes we get two slightly different viewpoints of the object, with a small displacement between the views. The human vision then combines the two images to estimate the depth of objects by matching up similarities and notice the differences [18], [19]. The general technique of imaged based 3D reconstruction is based on this idea, but here we can combine several images to create an entire 3D model. This way of using stereo vision to create a model from images is usually done using a method called Structure from Motion (SfM).

The benefits of using image based methods is that it is easy, fast and inexpensive. Also, a high resolution of the 3D model can be obtained if the original images are of good quality.

### 2.2.1.1 Structure-from-Motion

One method of calculating the 3D coordinates from two or more images is the SfM method [17], [18], [20]. Generally SfM takes a set of images and returns the camera parameters and a set of 3D coordinates. The camera parameters refers to the camera position and the inner camera parameters, such as focal length [17]. A SfM algorithm has the following pipeline [17], [20]:

1. Detect interest points, i.e. 2D features in every image.
2. Match 2D features between images.
3. Calculate 3D points and camera positions given the matching features.
  - (a) Estimate relative pose of two or more cameras.
  - (b) Do triangulation: estimate the 3D points given the matching features and the estimated camera poses.
  - (c) Estimate pose of new camera, and redo point (b).
4. Do bundle adjustment to globally optimize the obtained 3D points and camera parameters.

The features detected in the first step are usually distinct points such as edges or corners. A common algorithm for detecting and matching features is Scale-Invariant Feature Transform (SIFT). SIFT uses Difference-of-Gaussian (DoG) which chooses interesting points where we have extreme values. Then descriptors are created of the points which are used to match the features.

To minimize the number of incorrect matched features it is common to use Random Sample Consensus (RANSAC). RANSAC is an iterative way of fitting a model to a set of data points, thus minimizing the outliers. The triangulation in step 3(b) can also be done using RANSAC. Figure 2.5 shown the principle of triangulation, where  $C_i$  is the camera pose of image  $i$ ,  $x_i$  is the 2D feature and  $X$  is the triangulated 3D point.

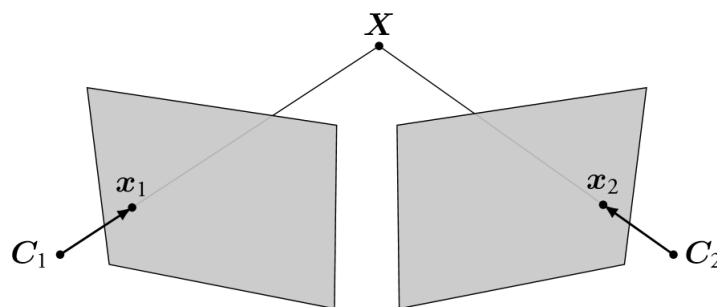


**Figure 2.5:** Illustration of how triangulation works.

As a last step in the SfM pipeline the bundle adjustment is used to refine the result by minimizing the reprojection errors, generally by using non-linear least square algorithms [17], [18], [20].

The SfM algorithm can either be done for a random set of images or having a

order between the images. Thus, when matching the features in step 2, this can be done for either all combinations of images or for only the connected images. For example, when taking a sequence of images it might be faster to only check the features of nearby images, but with the risk of missing matching features of other images. When the SfM algorithm has found all the corresponding matches, the output is the calculated 3D coordinates which is called a point cloud.

### 2.2.1.2 Multi View Stereo Algorithms

The SfM algorithm is an underlying method for the use of Multi-View Stereo (MVS) algorithms, which is a term used for techniques based on stereo correspondence and more than two images. The MVS algorithm is based on SfM since MVS assumes known camera parameters [17].

Since the MVS algorithms finds corresponding points between images it requires some distinct points in the images. This implies that the quality of the input image and the camera parameters affects the result of the 3D model [17], [18]. It is for example harder to reconstruct objects if the light in the image is bad or if the object has a reflective surfaces [18]. By using the SfM method we acquire a sparse 3D reconstruction usually as a 3D point cloud, therefore it is important to choose an appropriate MVS algorithm to make the model denser.

### 2.2.2 Active Scanning Methods

Active methods emits light, such as laser beams and infrared light, and measures the reflection of the object [8], [9]. Active sensors relies on artificial lights or patterned projections to measure the depth of an object. There are several techniques available and these can be based on, for example, triangulation using laser light, reflectively principles or time-of-flight [8].

The idea behind active sensors in 3D reconstruction is that it can be done in real time providing live feedback to the user. The process of 3D scanning with a camera is done by rotating the 3D scanner around an object, and in each step the sensor returns a depth map. Some scanners also returns a colour map, requiring that it has a camera capturing the corresponding colors. The obtained data can then be processed into a dense 3D reconstruction that is suitable for 3D printing, meaning that it has no holes and is segmented [16].

### 2.2.3 3D Reconstruction

For some passive and active methods it is common that the output 3D model has the form of a point cloud. A point cloud consists of the 3D coordinates, for example calculated using triangulation in the SfM algorithm. However, in many applications, such as 3D printing, it is more convenient to have the model as a surface. A 3D model can either be represented as a surface model, a solid CAD model or a polygon mesh.



**Surface model:**

The surface model represent the 3D object using mathematical curves or splines. An example of this is the Non-Uniform Rational B-Splines (NURB), which uses mathematical functions to represent a curve on the surface. Since a NURB curve is based on functions with control points, this makes it independent of resolution where it is unaffected if the model is scaled.

**CAD model:**

CAD models are instead based on designing objects using drawing in a CAD software. The objects can for example be drawn by combining shapes and lines in either 2D or 3D. A CAD model is easy to change and edit since it is based on the parameters of the shapes and lines.

**Polygon mesh:**

A polygon represents a surface using faces, vertices and edges. The faces are smaller, convex polygons, which is connected to the vertices by the edges [21]. The polygons are usually triangular since all polygons can be made into triangles [22]. A mesh contains a lot of data and is hard to edit. However, it is easy to change the resolution by increasing and decreasing the number of polygons, and to create specific details.

If the aim is to create a surface from a point cloud, the most common way is to use polygon meshes to represent the surface. Polygons can represent both a 3D surface and a solid 3D model, and is defined by the coordinates of the vertices and connective points. Another way to represent a solid 3D model is to use voxels. Voxels are the 3D equivalence to pixels of a 2D image and are, in contrary to polygons, defined by their position relative to other voxels.

### 2.2.3.1 Poisson Surface Reconstruction

Reconstructing a surface from a point set implies fitting the data, filling holes and remeshing the model. A well known technique for creating surfaces from point clouds is the so called Poisson Surface Reconstruction [23]. This method creates a water-tight surface from oriented point sets by reformulating the problem as a Poisson equation. This creates a solution which globally reconstructs a surface, in contrary to other implicit solution that divides it into regions and solves it locally. Poisson Surface Reconstruction is a method that approximates noisy data, thus creating a smooth surface.

The reformulation of the problem into a Poisson equation is done by firstly introduce a 3D indicator,  $\chi$ . This indicator has the value 1 if a point is inside the model and 0 if it is outside, see figure 2.6. Since the indicator is constant almost everywhere its gradient creates a vector field,  $\vec{V}$ , which is zero almost everywhere. The exception is for points near the surface, where the gradients is the inward pointing normals of the surface.

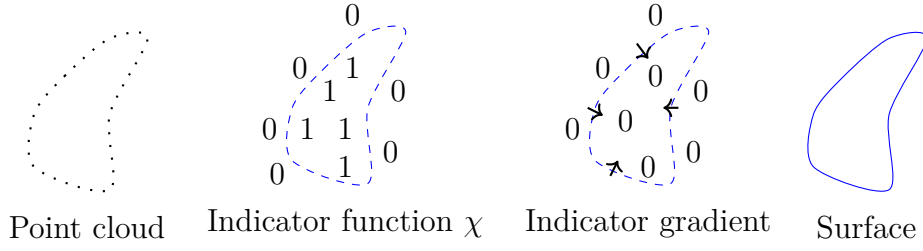


**Figure 2.6:** Illustrative image of how the Poisson Reconstruction processes an outward oriented point cloud to a surface, using an indicator function and an indicator gradient.

The oriented point set is now represented as the gradients of the indicator,  $\nabla\chi$ . The aim is then to find the best scalar function  $\tilde{\chi}$  that is closest to the vector field such that  $\nabla\tilde{\chi} = \vec{V}$ . By then applying the divergence operator the problems forms the Poisson equation,

$$\Delta\tilde{\chi} = \nabla \cdot \vec{V} , \quad (2.1)$$

where  $\tilde{\chi}$  is the estimated indicator function and  $\vec{V}$  is the vector field of gradients of  $\chi$ . This has transformed the original variational problem into a Poisson equation, from which a approximated least-square solution can be numerically calculated. Notice here that this formulation requires that the normals of the point set is oriented.

However, this original version of Poisson Surface Reconstruction has been updated due to it over-smoothing the data. The original version uses a global offset to adjust the implicit function thus making the average value zero, which causes problems when errors are present. Instead, a new version called Screened Poisson Surface Reconstruction has been developed, which explicitly interpolates the points [24]. By adding a penalty term,  $\alpha$ , when approximating the indicator function,  $\chi$ , this reduces the importance of fitting the gradient and the values. This can be interpreted as a screened Poisson equation similar as equation (2.1), resulting in

$$(\Delta - \alpha\tilde{I})\tilde{\chi} = \nabla \cdot \vec{V} , \quad (2.2)$$

where  $\tilde{I}$  is the identity matrix.

The Screened Poisson Surface Reconstruction algorithm has a number of parameters which can affect how the problem is solved. The main parameters to consider is the reconstruction depth, the interpolation weight and the minimum number of samples [24].

- *The reconstruction depth* indicates the maximum depth of the octree for the surface reconstruction. An octree is a branching tree which divides a space into eight subspaces, see figure 2.7. Indicating that a reconstructing at depth  $d$  means trying to solve the problem on a voxel with the maximum resolution of  $2^d \times 2^d \times 2^d$ . For example if  $d = 1$ , as in the middle figure in 2.7, this will solve the problem at a voxel with a resolution no larger than 8.

- *The interpolation weight,  $\alpha$* , specifies the importance of the explicit interpolation of the points. Setting  $\alpha$  to 0, indicates that the problem in equation (2.2) becomes the original Poisson Surface Reconstruction algorithm in equation (2.1).
- *The minimum number of samples* indicates the minimum amount of points that should fall within an octree node.

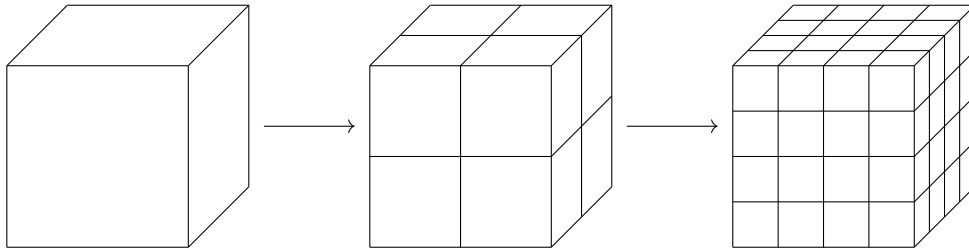


**Figure 2.7:** Image of two iterations of a octree where a voxel subdivides into octants, thus increasing the resolution of the voxel. Each square is a  $n$  octree node.

### 2.2.3.2 Poisson Disk Sampling

The application of the Poisson Disk Sampling algorithm is to sample points of a mesh or to subsample a dense point cloud [25]. By subsampling a dense point cloud the process of surface reconstruction becomes faster and the surface becomes smoother.

The Poisson Disk Sampling is based on a Poisson function which returns an integer random value with a probability of a Poisson distribution. The algorithm generates random samples onto the surface or the point cloud. The generated samples are checked to be within a minimum radius to each other, and the samples that violates this condition are removed, see figure 2.8. The result is an even but randomly subsampled point cloud[25].



**Figure 2.8:** Poisson Disk Sampling visualised on a bunny, where the distance between samples are viewed in a colour gradient [25].

## 2.3 Post Processing a Model

Often when reconstructing a 3D model of a real object using different scanning devices, unwanted noise is added to the data. By processing the model further the surface can be made smoother in order to remove outliers, or the resolution of the model can be increased or decreased. When post processing the model it is assumed that the obtained model is a polygon.

### 2.3.1 Smoothing of Surface

One of the first measures to improve a model is to smooth it. Smoothing is done to remove the noise while preserving the model as close as possible to the original object. One approach to surface smoothing is to use Laplacian smoothing [26]. In image processing Laplacian smoothing is done by replacing a point by the average of the adjacent points, see figure 2.9.

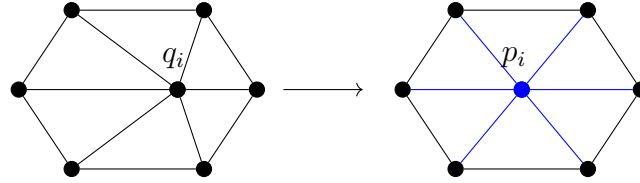


**Figure 2.9:** Laplacian smoothing, where a point is repositioned as the average of the adjacent points [26].

This means that the new position,  $p_i$ , of point  $i$  becomes

$$p_i = \frac{1}{N} \sum_{j=1}^N q_j ,$$

where  $j$  is the adjacent points to  $i$  with position  $q_j$ , and  $N$  is the number of adjacent points. Laplacian smoothing is simple to implement, but it has the disadvantage of causing the model to shrink. One way to decrease the degree of shrinking is to use HC-Laplacian smoothing [26]. The HC-algorithm seeks to push back the new position  $q_i$  to the original position  $q_j$  by creating an average of the difference of the adjacent points. Let  $b_i$  be the difference between  $p_i$  and  $q_i$ , then the average distance is

$$d_i = -\frac{1}{N} \sum_{j=1}^N b_j ,$$

where the position  $p_i$  is then mapped to  $p_i + d_i$ .

The HC-algorithm is a good way to smooth a mesh without the mesh shrinking too much. Smoothing algorithms can also be used to smooth point clouds. The idea is to create a mesh from the point cloud. This mesh is then smoothed, which also gives a smoothed point cloud. This first mesh does not need to be perfect, only similar to the original point cloud.

### 2.3.2 Simplification of Surface

One drawback of using polygon meshes is that the data for the vertices and edges requires a lot of space. Therefore it is beneficial to simplify the model by reducing the amount of polygons in a mesh, while preserving the surface as much as possible. Here it is a trade off between space and computational time versus resolution of the model, where the resolution of the model can be represented at different Levels of Detail (LOD). Simplification of polygons can either be done by iteratively removing the mesh elements one at the time or by processing the entire mesh in one step [21], [27].

The iterative methods assigns a cost to each element, removes elements with the lowest cost and then re-triangulates the area with the hole [21], [22], [27]. Here the mesh elements can refer to either a face, edge, vertex or a patch of faces. What distinguishes different iterative methods is how elements are removed (local operator) and which elements to remove (error).

The most common local operators is edge collapse or vertex decimation [21]. Vertex decimation removes a vertex and then tries to fill that hole by creating new triangles. Edge collapse either removes the edge between two vertices or removes an edge with one connecting vertex. This creates a hole which is filled by creating new triangles, see figure 2.10.

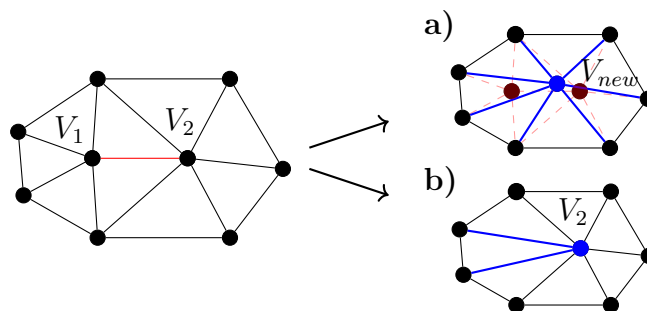


**Figure 2.10:** Two versions of edge collapse. **a)** Edge collapse by removing two vertices and replacing it with a new. **b)** Edge collapse by removing one vertex and re-triangulate.

The error is used to decide which element to apply the operator on, and can be calculated either locally or globally. One local method is the quadric error metric which measures the error as the distance from a vertex to the supporting planes connected to that vertex. One global method used is the Hausdorff distance, which calculates the distance between two point sets [21]. The Hausdorff distance is explained more further down in section Hausdorff Distance.

The methods of simplifying the entire mesh in one step are generally not as accurate as the iterative methods. However they are instead much faster and very easy to implement [21]. Here the most common algorithm is vertex clustering. Vertex clustering assigns a weight to each vertex declaring how important that vertex is.

The input mesh is then divided into 3D cells, voxels, according to a given resolution. In each cell only the most important vertex is kept, and all the other vertices are clustered to this vertex. Thus a simplified mesh is obtained.

### 2.3.3 Subdivision of Surface

The subdivision of a surface is usually applied to increase the number of triangles of a mesh, and thus increasing the resolution and creating a smoother surface. One approach to subdivide the surface is the Least Squares Subdivision Surfaces (LS3), which iteratively projects each vertex onto an approximation of the polygonal mesh [28]. The function can take a coarse polygonal mesh and produce a smooth surface through this iterative process, see figure 2.11.

In the first step of the LS3 function a splitting rule is applied to the meshes to obtain a denser mesh, in the second step a relaxation rule regularises the mesh and in the third step each vertex is projected onto its least-squares approximation. The LS3 has the ability to remove ripples and other subdivision artifacts.

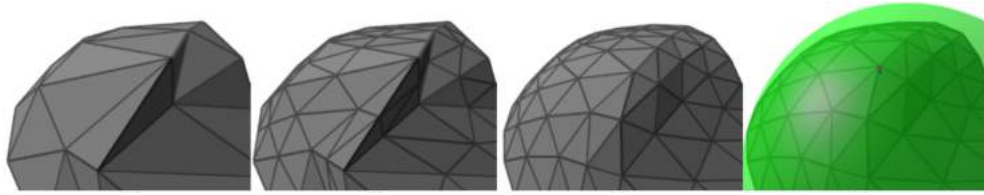


**Figure 2.11:** Illustration of the iterative process of LS3, by first triangulate each polygon, relax the mesh and then project it using least-square (seen as green) [28].

## 2.4 Comparing Models

When a model has been obtained, the quality of that surface can be evaluated by comparing the surface to either another surface or a point cloud. The ideal case is to compare the surface to the ground truth, which sometimes can be hard to obtain of the real model. One way of comparing models is by analyzing the geometrical distance between two surfaces. The geometrical error can be measured either by considering local or global changes [21].

### 2.4.1 Hausdorff Distance

Hausdorff distance can be used as a way of globally comparing the geometrical distance between two surfaces [29], and is a well known method of measuring geometrical errors [21], [22]. The main application is to compare a surface and its simplified version to see how well a simplification algorithm works for different Levels of Detail. It can also be used to see how well two different algorithms reconstruct a surface from a point cloud, or how well two methods reconstruct a 3D model.

To compute the geometrical difference the measurement is based on an error distance defined on the approximation of the surface-to-surface distance. The measurement is done by firstly sample the surface for a chosen sample resolution and secondly calculate the point-to-surface distance for each sample. Here, a distance between the surface  $S$  and the point  $p$  is described as

$$e(p, S) = \min_{p' \in S} d(p, p') , \quad (2.3)$$

where  $d()$  is the Euclidean distance between two points. The one-sided distance between two surfaces  $S_1$  and  $S_2$  is then declared as,

$$E(S_1, S_2) = \max_{p \in S_1} e(p, S_2). \quad (2.4)$$

The Hausdorff distance is then the two-sided distance defined as the maximum of  $E(S_1, S_2)$  and  $E(S_2, S_1)$ . Note that the definition of  $E$  is not symmetric. If the surface is oriented a signed distance can be introduced to distinguish between positive and negative distances, indicating that a point has a positive distance if it lies outside a surface and negative distance otherwise, see figure 2.12.

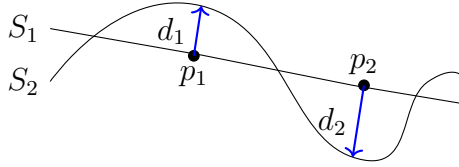


**Figure 2.12:** The signed distance of the Hausdorff distance, where  $d_1$  is positive and  $d_2$  is negative, assuming that the surfaces  $S_1$  and  $S_2$  has normals upwards.

## 2.5 3D Printing

3D printing is a technique that manufactures 3D objects by depositing a certain material layer by layer and can also be called additive manufacturing [30]. There are several benefits of using 3D printing, such as making a product on demand, custom making a design or building complex geometries that can not be made with other manufacturing methods. On the other side, 3D printing has the drawbacks of a high printing cost, limited building volume and limited material variety [30], [31].

An example where additive manufacturing is beneficial is when it comes to personalized products, such as medical implants and especially orthopedic implants [32]. When creating an orthopedic implant, the implant is designed using CT or MRI images. From these images a bone model can be reconstructed, which helps designing the implant and aids the surgeon to place the implant at the correct location. With the use of additive manufacturing this process can become more time efficient and facilitate the designing of the implant.

The 3D printer also needs a model to print, and this can be obtained either using CAD, 3D scanner or a digital camera together with stereo vision algorithms.

The obtained 3D model is usually represented as a polygon mesh or a CAD model. These parts were deeper explained in section 3D Reconstruction and Modelling.

Figure 2.13 illustrates the process from an object to model, which then is printed. The previous sections explained the first step from an object to a 3D model. This section will explain the steps from a model to a printed object.



**Figure 2.13:** Overview of the steps from a real object to the printed object.

### STL-file

The obtained polygon mesh or CAD model needs to be converted into a suitable file format. Most additive manufacturing techniques use Stereolithography (STL) files as the standard format [31]. However, there exists many other file formats that can represent a 3D model, such as Object (OBJ) or Polygon File Format (PLY), but not all 3D printers can handle these formats.

The STL file represents the surface using triangles, and consists only of vertices and the normal declaring the outward face of the triangle. This is a very simple format, which contains no other information than the geometrical surface. Other file formats, e.g. OBJ or PLY, can also store parameters such as color and texture. The benefits of using STL format is that it is easy to repair. This might be necessary, since a model needs to be waterproof, i.e. no holes in the structure, before printed.

### G-code

Since the 3D printer manufactures an object layer by layer, the STL model needs to be processed in a slicer software. The slicer software takes the 3D model and slices it into 2D layers. For the 3D printer to understand this, a certain code is generated which the printer can read, this code is generally called a G-code. A G-code is a general language consisting of commands telling the 3D printer which coordinates to print, which material to use, how fast to print and how much to print. However, some printers use their own code for printing, but most codes are very similar.

As mentioned, a model needs to be waterproof in order to be printable. Another condition is that the model needs to be stable. Depending on the material, parts of the model with an high angle will collapse when printed. To prevent this, support material can be added in the slicer program, which works as pillars to support hanging parts. The stability also depends on how much of the inside of the model that is filled. If the infill density is high the model becomes stable, but it will take longer time to print.



Another important parameter is the layer height. By changing the layer height the resolution of the model is changed. A small layer will increase the resolution, but this will also take longer time to print.

## Additive Manufacturing Technologies

There are several techniques used to 3D print an object. For example, the material can be extruded using melting or pressure. The material that is printed can be polymers, metal, ceramic or any other material suitable for printing [30]. Some printers can even print using two different materials or different colors of the same material.

Some more common printing processes is Stereolithography (SLA), Selective Laser Sintering (SLS), Fused Deposition Modeling (FDM) and Inkjet printing.

- SLA is a printing technique that uses ultraviolet light that causes chains of molecules to link together, forming polymers [33].
- SLS uses laser to sinter powdered material by aiming the laser at points, which causes the material to bind together [34].
- FDM melts material that is unwound from a coil to supply the material layer by layer [35].

### 2.5.1 3D Bioprinting

The term 3D bioprinting refers to the use of additive manufacturing to accurately deposit living cells, biological materials and biochemicals into chosen geometries [36]. Bioprinting is an application used within tissue engineering, where it has the potential to print tissues and organ-like structures [37]. To be able to print cells a so called *bioink* is used, which usually consists of proteins and polymers [38]. The bioink provides a hospital environment and a mechanical support in which the cells can attach to and proliferate in. One example of a supportive material is hydrogels, which are polymeric networks that contain a high amount of water [39].

The most common printing techniques in bioprinting is the inkjet [40], microextrusion and laser-assisted printing [36], [38].

- Inkjet printing is a system that creates pressure to eject small droplets of ink via the nozzle head. This drop-by-drop technique gives the illusion of an even flow.
- Microextrusion printing uses pneumatic or mechanical control to extrude an even flow.
- Laser-assisted printing focuses a laser on the printable material, which generates a small pressure bubble that drops onto a collecting substrate.

When bioprinting the most important factors to consider is the surface resolution, the cell viability and the biological materials used for printing. When choosing a biological material there are some features that is interesting to look at, such as

printability, biocompatibility and mechanical properties. Meaning that you want a material that is easy to print, that it should not create unwanted responses from the host and that the mechanical properties should match your need [36].

# 3

## Methods

### 3.1 Data Acquisition

The data for the models was collected using three different devices: digital camera, advanced 3D camera and a 3D scanner. The object to be modelled was a mannequin in plastic, visualizing the bust of a human. The mannequin did not have any hair.

#### 3.1.1 Digital Camera

The camera used was a system camera of model Nikon D40. The system camera was used with two different lenses, one ordinary lens (AF-S DX Nikkor 18-55mm f/3.5-5.6G ED II) and one macro lens (Tamron AF 70-300mm f/4-5.6 Di LD Macro 1:2). The ordinary lens is a kit lens that comes with the camera. The macro lens, compared to the kit lens, gives higher quality in the images such as improved sharpness. The macro lens is only in the telephoto focal range with a focal length between 180-300mm. See table 3.1 for specifications of lenses, resolution, focal length and aperture.

Camera	Resolution (megapixels)	Lens	Focal range	Aperture
Nikon D40	6 MP	DX Nikkor	18-55mm	f/3.5-5.6
Nikon D40	6 MP	Tamron Macro	70-300mm	f/4,0-5,6

**Table 3.1:** Table of the digital camera used, and the two different lenses. The MP stands for megapixel, the focal range indicates the interval of the focal length and f is the maximum aperture.

##### 3.1.1.1 Image Acquisition

When taking the images some steps was followed to acquire a good model. Notice that the image acquisition was not made in a controlled studio environment. The steps:

1. The mannequin was placed on a pedestal or table.
  - (a) For some cases the pedastal was covered with newspapers to get a unique background.
2. The mannequin was pretreated before taking the images. This was done by adding make-up to mimic skin and adding a beanie to hide the large, smooth surface of the head.

3. A sequence of images was taken in a sector of a circle around the mannequin. The sector had degrees between 120°-360°.
  - (a) Each sequence of images was taken with a high-overlap, aiming for a 70-90% overlap. The percentage of the overlap was roughly estimated by considering the amount each image had in common and the amount of images over a distance.
  - (b) A large number of images was taken in order for the MVS algorithm to work better.
  - (c) The focal length and the resolution stayed the same throughout a sequence.
  - (d) The lighting was of the scene was consistent, natural and bright. No flash was used.
  - (e) The background was not controlled, but uniform background and backgrounds with a repeating pattern was avoided.
4. The images was not processed before uploading and reconstructing the model.

When acquiring images, four versions of acquiring images was tested, with different combinations of parameters described above. These versions can be seen in table 3.2.

Version	Lens	Focal length	Camera trajectory
1	Macro	70mm	120°, 3 layers
2	Macro	70mm	180°, 3 layers
3	Ordinary	38mm	270°, 3 layers
4	Macro	185/195mm	360°, 1 layers

**Table 3.2:** Table over different tests taken under different conditions, with different setups. Version 1: Macro lens with low focal length, Version 2: patches, Version 3: unique background, Version 4: Macro lens with high focal length.

#### 3.1.2 Advanced 3D Camera

The advanced 3D camera was a *static-3dMD system*, specially made by the company 3dMD [41] for Sahlgrenska University Hospital in Gothenburg. The system consist of a booth made up by four walls with nine cameras positioned around the center, see figure 3.1. The system can image the upper body in 360 degrees.

The object to be imaged is positioned in the centre of the booth, in the cross section of the nine cameras. The 3dMD system then sends out a flash of a patterned light, retrieving images from all angles at a capture speed of 1.5 milliseconds. The pattern from the flash helps the system to triangulate a polygon mesh with the correct scale. The system also saves the color of the object from the camera images.

#### 3.1.3 3D Scanner

The 3D scanner used was *HandyScan3D* from the company Creaform [42]. The HandyScan 3D (HS3D) is a portable hand held laser scanner that sends out a laser

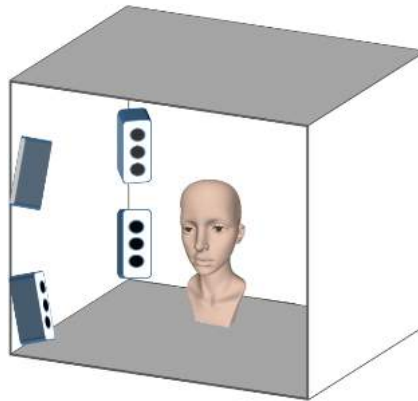


**Figure 3.1:** Illustration of the static-3dMD system, using 9 cameras evenly distributed around the center, capable of imaging 360 degrees of the upper body.

grid and uses triangulation on optical reflectors (reflective targets) to determine its relative position to the object.

The mannequin is prepared by positioning the reflective targets, i.e. round adhesive dots, randomly around the entire object. The dots were placed close enough for the HS3D to detect at least 3 dots within the laser grid, but not closer than 20 mm between each dot. The mannequin is then scanned by moving the laser grid over the object until the entire object is modelled. The surface rendering of the object can be seen in real time when scanning.

The accuracy of the scanner can be up to 0,030 mm, and the resolution can be up to 0,05 mm. The output was a ready mesh or a point cloud of the object with 0.1 mm resolution.

## 3.2 3D Modelling

For the 3dMD and the HS3D methods, a 3D model is generated directly in the belonging software. However, the images from the digital camera need further processing to get a 3D model. The 3D model was made in two main steps, by creating the dense point cloud from the images and then reconstructing a surface from the point cloud.

### 3.2.1 Dense Point Cloud

The dense point cloud was created using an open source software called `visualSFM` [43], [44]. The point cloud was then generated using the following steps:

1. Upload the images.
2. Compute the matching SIFT points between the images
3. Compute the sparse reconstruction from the computed matches, creating a sparse point cloud

4. Run dense reconstruction with chosen MVS algorithm, creating a dense point cloud

The chosen MVS algorithm was the Patch-based Multi-View Stereo (PMVS) algorithm developed by Furukawa and Ponce [45]. The dense point cloud was then manually cleaned by removing points that was obviously outliers.

#### 3.2.2 Surface Reconstruction

The surface reconstruction and the post processing was done using the open source software **Meshlab** [46]. The surface reconstruction of the point cloud was done using the method *Screened Poisson Surface Reconstruction*. Some main parameters was considered with the following values:

- The reconstruction depth: This value was set between 10-12. A higher value gives more accurate reconstruction, but this also considers the noise. Default value: 8.
- The interpolation weight,  $\alpha$ : Values between 0-4. A lower value gives a smoother result. Setting  $\alpha$  to 0 means solving the problem as an unscreened Poisson Reconstruction. Default value: 4.
- The minimum number of samples: 1-5 or 15-20. For noise-free data this value should be small, between 1-5. For noisy data it should be larger, between 15-20, to provide a smoother reconstruction. Default value: 1.5

Different combinations of values was tested for these three parameters, the values used can be seen for Version 1-4 in table 3.3. In Version 1 the macro lens was used with a high overlap and a unique background. In Version 2 distinct points was added to the mannequin by using multiple adhesive patches. Version 3 was taken similar as Version 1, but with an ordinary lens and a unique background in the form of newspapers. Version 4 was taken 360° around the mannequin. All of the versions, except Version 4, was taken in the form of a serpentine of three layers (i.e. two turns), with the focus on the face. If the point cloud was not oriented, the normal of

	Reconstruction depth	Minimum Nr. of samples	Interpolation weight $\alpha$
Set 1	12	1.5	4
Set 2	12	1.5	1
Set 3	12	20	4
Set 4	8	1.5	4

**Table 3.3:** Table over the values of different parameters used to reconstruct the model.

the points was computed before doing the Screened Poisson Surface Reconstruction.

Before doing the surface reconstruction the point cloud was sometimes sampled using *Poisson Disk Sampling*, which was done when the point cloud was either very dense or contained a lot of noise. After the reconstruction the model was further processed by smoothing, simplifying or subdividing the mesh.

### 3.3 Comparing Models

When comparing the obtained models an open source software called **CloudCompare** was used. The two surfaces was firstly aligned to each other and then the geometrical distance was calculated.

The models was aligned by manually choosing at least 3 equivalent points in each model, from which a transformation matrix is calculated. If the difference between the two models were small, an automatic registration was instead used. This is done using an Iterative Closest Point (ICP) algorithm to compute the transformation matrix.

CloudCompare compares two surfaces using a nearest neighbour approach, which is similar to the Hausdorff distance. The output is a visualization of the error, which uses a color scale to indicate different distances. The output also includes values of the average, minimum and maximum distances. Meshlab can also compare two surfaces and use one-sided Hausdorff distance, which gives the output in numbers. However, CloudCompare is designed for comparing point clouds and therefore suits better for this purpose.

### 3.4 3D Printing

When 3D printing, the polygon mesh model of the mannequin obtained from the HS3D was used to create a mask of the face. This face mask was then printed in thermoplastic Polylactide (PLA) and in Celullose Nanofibrils (CNF).

#### 3.4.1 CAD Design

When designing the face mask from the mesh model, a CAD software called **Rhinoceros** was used. This model of the entire mannequin was processed into a face mask in the form of a shell following the face of the model.

#### 3.4.2 3D Printer

For printing the plastic face mask the 3D printer **MakerBot Replicator 2** was used, see figure 3.2. When preparing the model before printing the slicer program, **MakerBot Desktop** was used for MakerBot. When preparing the file the following parameters was mainly considered: layer height, infill density, infill patters, extrusion speed and support structure.

The face mask was printed using PLA filament. The parameters for printing with Makerbot was a linear infill pattern, an infill density of 100% and a layer height of 0.1mm (resolution).

#### 3.4.3 3D Bioprinter

For printing the face mask the 3D bioprinter **Inkredible** and the open source slicer program **Slic3r** was used. The face mask was printed with CNF, and with Nivea cream as support structure. The parameters used for printing the face mask was a infill density of 40% using concentric lines and a layer height of 0.35mm for the nanocellulose and 0.5mm for the Nivea cream. The extrusion speed was set to 20 mm/s for the infill material, 60 mm/s for the support material and 10 mm/s for the perimeters (the outer shell of the infill).

Before printing, two syringes was filled, one with CNF and one with Nivea cream. When filling the syringes it was important to keep it free from air bubbles. These bubbles can cause clogging when printing. The default pressure was 110 Pa for nanocellulose and 55 Pa for Nivea cream, which was determined from testing where the materials have an even flow and printing. The pressure may then be altered during printing.

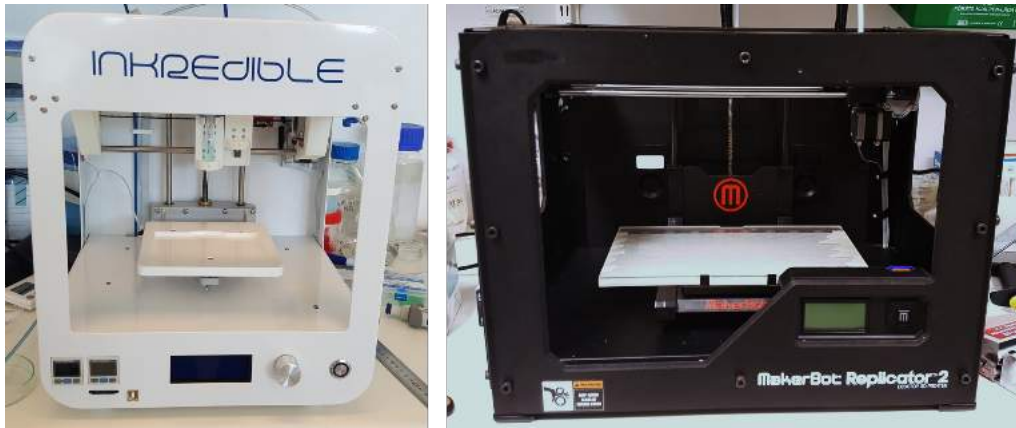


**Figure 3.2:** The Inkredible 3D bioprinter and the 3D printer MakerBot Replicator 2.

##### 3.4.3.1 Printability Analysis

The printability analysis was done to see how the materials behave when printing. The analysis was done by firstly deciding at which pressure the material flows evenly. This was done by weighting the mass after letting the material flow for 20 seconds. This was done three times for different pressures. The nanocellulose was tested for the pressures of 100 Pa, 105 Pa and 110 Pa. The Nivea cream was tested for pressures of 55 Pa and 60 Pa. Each pressure was printed three times, from which an average of the weight was taken. The chosen pressures were determined around the default pressure, where the materials are known to have an even flow.

The next step was to see how the material behaves when printed at different printing speed. This was done by printing the material in a 120 mm long pattern using varying extrusion speeds between 1.7-40 mm/s, where the pressure was constant. The pressure was set to 110 Pa for nanocellulose and 55 Pa for Nivea cream. Each



printing speed was printed three times and weighted between each time, from which an average weight was calculated.

The printed line was then assumed the form of a half circle with unknown radius,  $r$ , and a known length,  $l$ , of 120 mm. Using the formula of a half circle and the measurements above, the radius was calculated for each printing speeds. The volume of the entire printed line is,

$$V = \frac{\pi r^2 L}{2}. \quad (3.1)$$

The radius was then calculated as

$$r = \sqrt{\frac{2m}{\pi \rho l}}, \quad (3.2)$$

where  $m$  is the mass of the printed line and  $\rho$  is the density of the material. Since the material is nanocellulose, which mainly contains water, the density was set to 1 g/ml.



# 4

## Results

### 4.1 3D Modelling

The 3D modelling was done using three different techniques: digital camera, advanced 3dMD camera and HandyScan 3D (HS3D). In this section the result from the digital camera will be analyzed firstly, and secondly the 3dMD camera and the digital camera will be compared towards the HS3D. The HS3D is considered as a model close to the ground truth.

#### 4.1.1 Digital Camera

The acquiring of images was done by analyzing a set of chosen parameters. By changing the background, number of images and adding distinct points in the images, the quality of the model changes. The different versions that was tested can be seen in table 4.1 and 3.2. The tables lists the various sets of parameters used in each version.

	Camera trajectory	Nr. of Images	Overlap( $\pm 10^\circ$ )
Version 1	120°, 3 layers	86	88%
Version 2	180°, 3 layers	117	89%
Version 3	270°, 3 layers	140	86%
Version 4	360°, 1 layers	73	70%

**Table 4.1:** Table over different version of acquiring images of the mannequin using different conditions, with different setups.

Version 1 and 3 was imaged with a more unique background, while Version 2 instead had unique patches attached to the face of the mannequin, see figure 4.1. Version 4 was the only case which was taken with 360° around the mannequin. In the other three versions the camera trajectory had the form of a serpentine with two arcs and three layers, see figure 4.2.

From the images a sparse point cloud is created using Structure from Motion (SfM) and then a dense point cloud is created using a Multi-View Stereo (MVS) algorithm. This can be seen in figure 4.2, where the camera trajectory of a three layered serpentine was used. The point cloud is then reconstructed into a surface using screened Poisson Surface Reconstruction. When doing this three parameters was mainly investigated, the reconstruction depth, the minimum number of samples and



**Figure 4.1:** Version 2 where adhesive patches has been added to create distinct points on the surface of the model.



**Figure 4.2:** To the left is the sparse point cloud and to the right is the dense point cloud obtained of Version 1 using a SfM algorithm and then a MVS algorithm.

the interpolation weight  $\alpha$ . The default parameters chosen here is a reconstruction depth of 12, a minimum number of samples of 1.5 and a interpolation weight  $\alpha$  set to 4. Table 3.3 displays the four sets of values of the parameters that was used. If nothing else is mentioned the default parameters are used, otherwise one of the sets in table 3.3 is mentioned.

In figure 4.3, we see the process from image, to a point cloud which then is reconstructed into a surface using default parameters. Here we see how the reconstructions creates a surface by interpolating the points. With the default parameters the face gets a rough surface, and some bigger holes is located at the chin and the cheek. Also, the eyes is not very detailed and the eyelashes is completely missing.

Considering the dense point cloud in figure 4.3, most of the points are located in the face. This is a result of that the images are taken with the face in focus, as seen in figure 4.2. The neck, the beanie and the back of the head is only visualized in a few of the images. Therefore the resulting point cloud do not contain many points in these areas.

By applying the default reconstruction parameters to version 1-4 in table 4.1, the difference between the versions can be viewed. The result is shown in figure 4.4, and here one can see that all version has outliers to some degree. By doing a subjective evaluation, Version 1 (to the left) gave the best result with fewer outliers. However,



**Figure 4.3:** The process from image, to a point cloud and then a reconstructed mesh, with and without color. Bigger holes are circled in red.

Version 3 gave an overall good result where even the neck was modelled, which probably is because of the unique base of newspapers and the the high amount of images. Version 4 (to the right) gave the worst result, which is due to the low number of images taken and the low overlap. By only viewing the obtained meshes it seems as adding distinct points in the images give a better result. Both when adding distinct points in the background (newspaper) in Version 3 and when adding patches onto the mannequin as in Version 2.



**Figure 4.4:** From left to right, version 1-4 reconstructed using default parameters.

#### 4.1.1.1 Processing Comparison

As noticed in figure 4.4, modelling a smooth, uniform surface such as skin, results in outliers. By testing different sets of parameters in the reconstruction process, in table 3.3, one can see that the model can get a smoother surface. The different meshes obtained with different sets is compared to the model obtained from HS3D. To be able to compare the image based models to the scanned model, the point cloud is aligned to the mesh, see figure 4.5.

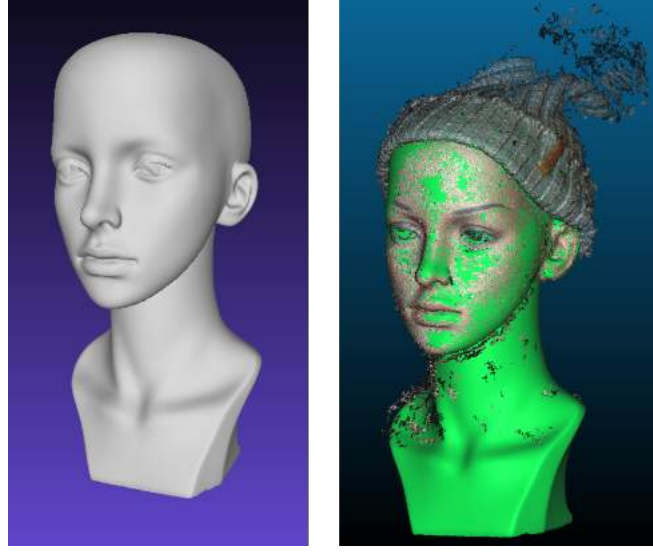


**Figure 4.5:** The mesh obtained using HS3D to the left, and the point cloud from Version 1 aligned to this mesh.

In figure 4.6 the point clouds from Version 1 and Version 2 is compared to the "ground truth" from HS3D. The models has a color scale indicating the distance from the point cloud to the reference model, HS3D. A value close to zero means that we are close to the reference mesh. For example, the beanie is colored red according to the color scale, which corresponds to a high distance from the point cloud to the mesh.

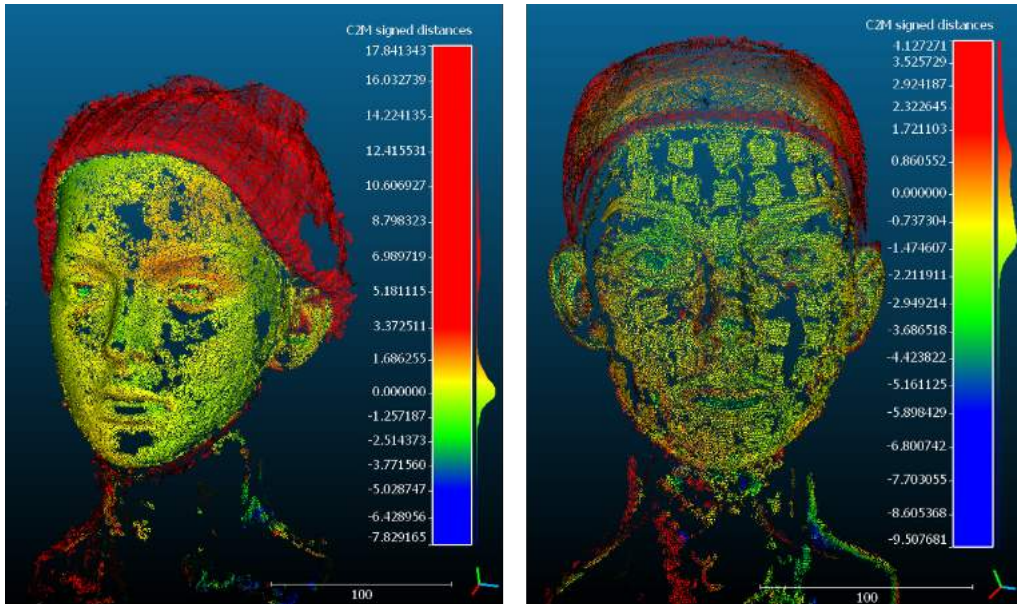


**Figure 4.6:** The point cloud from Version 1 and Version 2, to the left and right respectively, compared to the mesh obtained using HS3D. The models has a color scale indicating the distance from the point cloud to the reference model.

Notice that, in figure 4.6, the patches in Version 2 has a high concentration of points with distances close to zero. Outside of these patches, the points are less concen-



trated and contains more outliers. This indicates that using distinct points can improve the point cloud. However, the result of Version 2 is similar to the Version 1 without patches, to the left. In Version 1, the points have a high concentration in the entire face with the exception of some holes. Nevertheless, overall it seems like the patches increases the possibility to get a good model.

One way of analyzing the point clouds further is to only compare the faces and neglecting the surrounding points. In figure 4.7, only the face of Version 2 with patches has been compared to the point cloud of HS3D. Here two point clouds is compared, instead of comparing surface-to-surface or point-to-surface.

To the left in figure 4.7 the difference in the distances are compared using a nearest neighbour approach, but since the point cloud is sparse the nearest neighbour is far away. To the right a local model has been used to get a more accurate comparison. In the point cloud where the local model has been used, we can see more clearly that the patches have distances close to zero, which are colored blue. This confirms the theory that using distinct points on the model gives a better result.

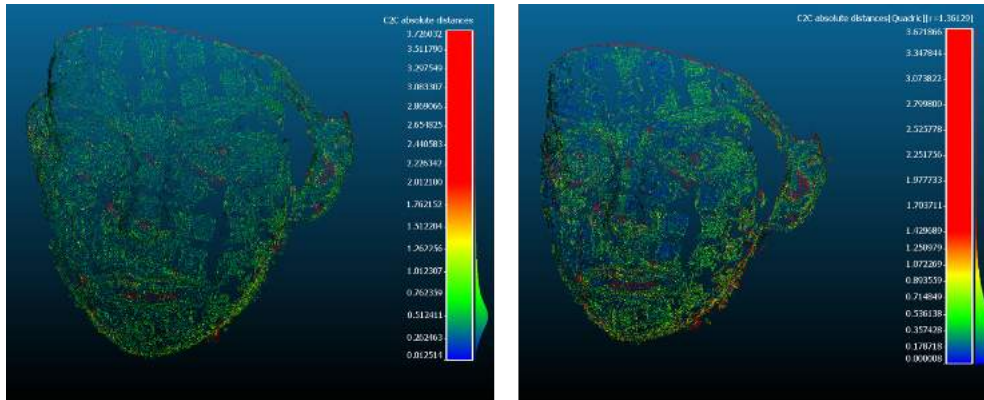


**Figure 4.7:** The point cloud of the face of Version 2 compared to the point cloud obtained using HS3D. To the left is a nearest neighbour comparison while to the right is a local comparison.

As mention, Version 1 gave a good result with fewer outlier. However, the surface is still rough. Therefore, the Version 1 mesh was smoothed using HC-Laplacian smoothing, where the comparison to the HS3D is seen to the right in figure 4.8. When comparing Version 1 with and without smoothing, it is noticed that that the smoothed face has a more even transaction from different distances (from yellow to green). However, it is hard to say that the smoothed face is better than the not smoothed mesh based on the distances. Using subjective opinion, one can conclude that the smoothed mesh probably best mimics skin.

Using a high reconstruction depth gives a more detailed mesh. When using a lower reconstruction depth, as with Set 4 in table 3.3, this gives a more smoother mesh. Version 1 with Set 4 is compared to the smoothed Version 1 with Set 1 in figure 4.9. The lower reconstruction depth of 8 gives a very similar result to using a depth of 12 and then do smoothing.

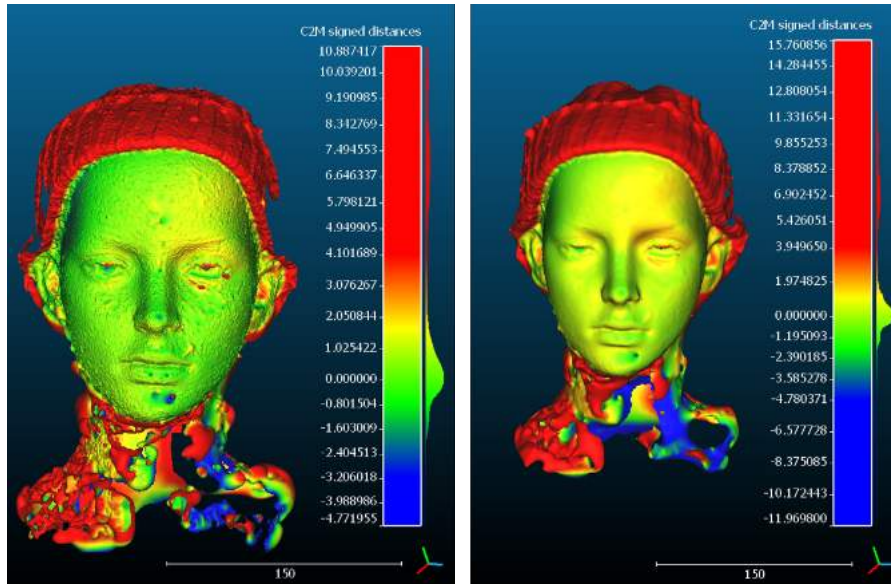


**Figure 4.8:** The mesh from Version 1 with parameters of Set 1, to the left, and Version 1 with Set 1 that has been smoothed, to the right. The meshes have been compared to the mesh obtained using HS3D. The models has a color scale indicating the distance from the point cloud to the reference model.

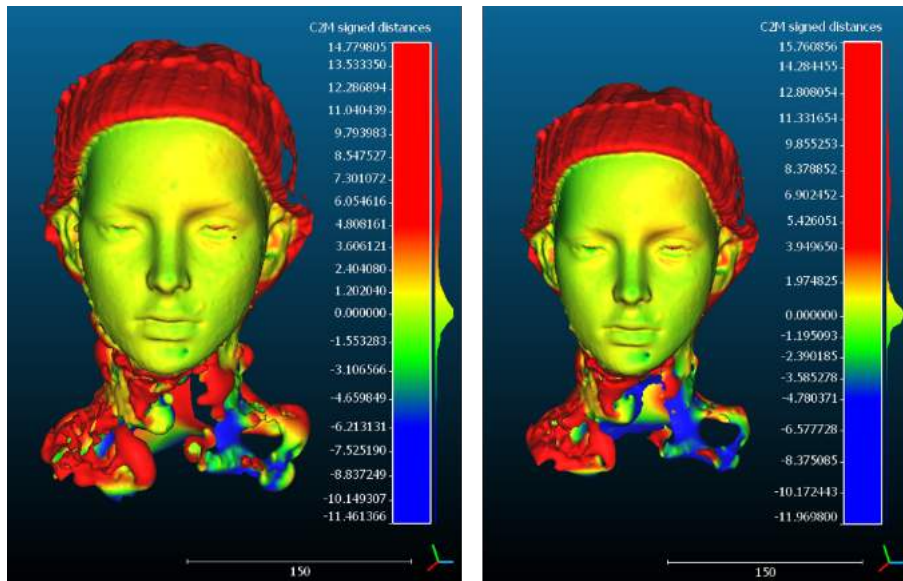


**Figure 4.9:** The mesh from Version 1 with Set 4 to the left, and Version 1 with a smoothed Set 1 to the right. The meshes has been compared to the mesh obtained using HS3D. The models has a color scale indicating the distance from the point cloud to the reference model.

Another idea of removing the outliers is to sample the point cloud. To the right in figure 4.10 Version 1 has been sampled using Poisson Disk Sampling and compared to the HS3D. Notice that the sampled point cloud has an even color over the face, with distances close to zero, compared to the original point cloud which varies in



the colors. The idea with sampling is to mainly reduce a dense point cloud, thus making it easier to process. However, the sampling also seems to create a smoothing effect on the point cloud.

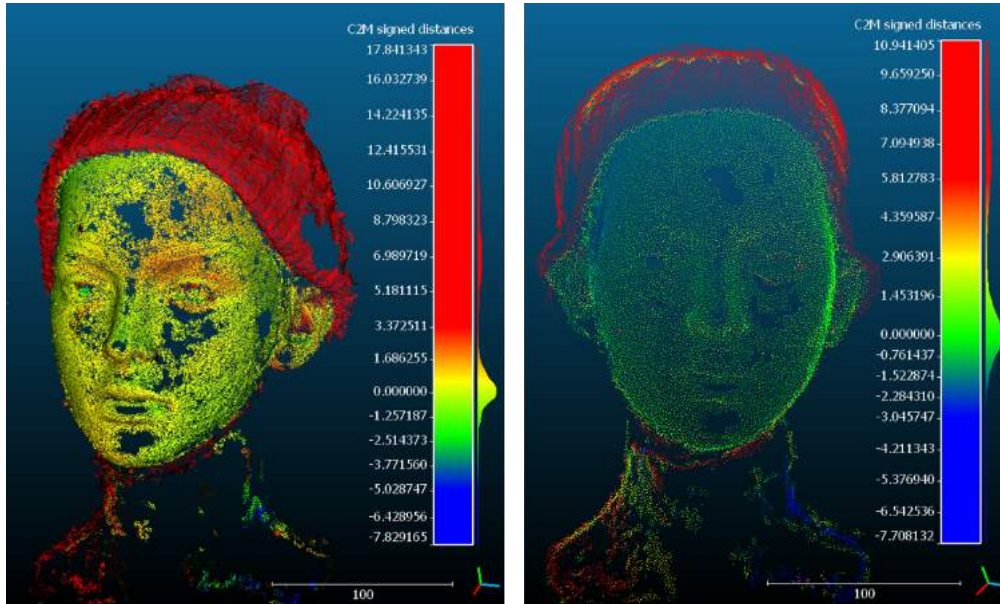


**Figure 4.10:** The point cloud from Version 1 to the left, and the sampled point cloud of Version 1 to the right. The point clouds has been compared to the mesh obtained using HS3D. The clouds has a color scale indicating the distance from the point cloud to the reference model.

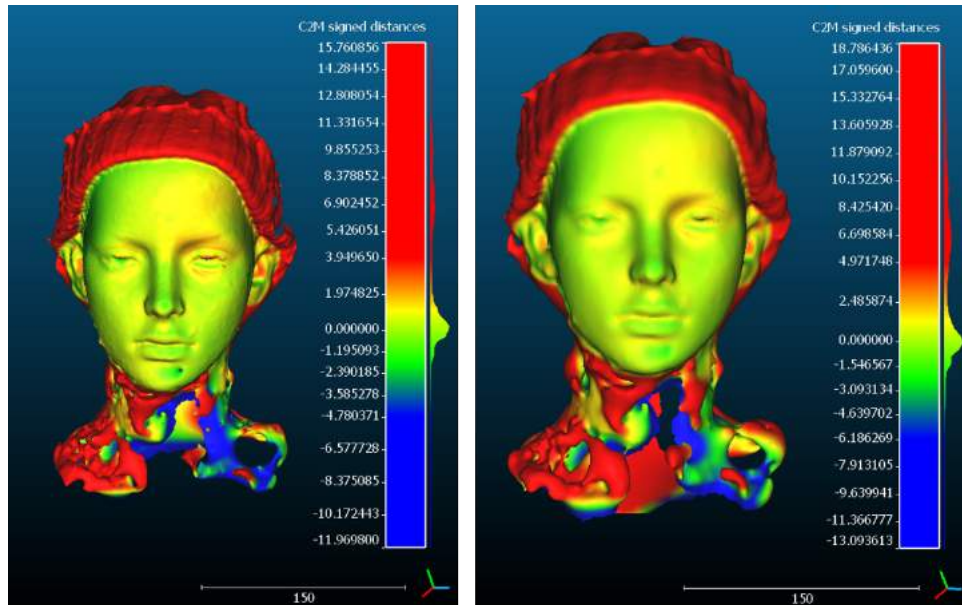


**Figure 4.11:** The mesh from the smoothed Version 1 with Set 1, to the left, and its mesh from the sampled point cloud with Set 1, to the right. The meshes has been compared to the mesh obtained using HS3D. The models has a color scale indicating the distance from the point cloud to the reference model.

When doing the same comparison, but with the reconstructed meshes instead of the point clouds, in figure 4.11, the difference can be seen more clearly. The sampling reduces the hole on the chin, which is colored with blue and circumscribed. On the other hand, by using sampling the details are also reduced, as can be seen especially around the eyes.

As a conclusion there are three ways to remove, or smooth over, outliers: by using sampling on the point cloud, choosing appropriate values for surface reconstruction (changing one or all of parameters), or by using a smoothing algorithm. Of course, other methods exist, but these are probably some of the simpler approaches. However, the best approach is to have high quality of the images and a point cloud that is generated correctly from the SfM and the MVS algorithm.

### 4.1.2 Method Comparison

The model of the mannequin obtained using the 3dMD camera can be seen in figure 4.12. Here the different camera angles are shown and how the pattern of the flash is designed. To the right the resulting mesh is seen, which has missing structures in the lower regions of the neck. This is due to how the mannequin is positioned in the booth. The object in the booth needs to be positioned correctly so that the flashes are not shown in any images. If the flashes are caught in the image, the mesh will probably contain holes and noise.

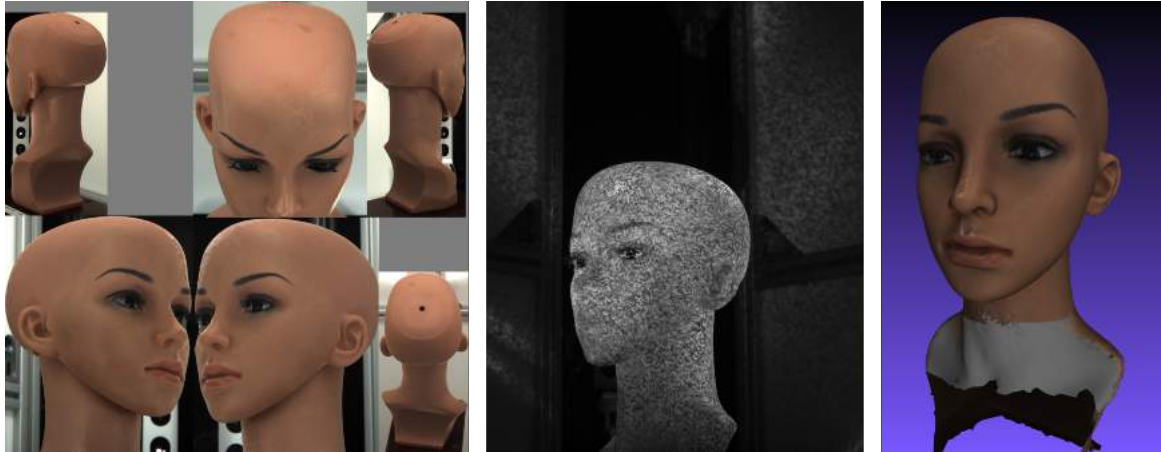


**Figure 4.12:** The process for the 3dMD camera at Sahlgrenska, showing the angles of images of the mannequin, the patterned flash and the resulting mesh.

The comparison of the model from the 3dMD camera to the model from the HS3D scanner can be seen in figure 4.13. Notice that the larger distances, in blue and red, are located in the lower region due to the problem described above. Instead, in the face the distances are very close to zero, with values between -1.3 to 1.3 mm. Since neither of the methods are good at imaging shiny, reflective objects there are some larger errors around the eyes, where it shifts in orange. However, overall the two methods give similar surfaces for the face. One problem with the 3dMD camera is the ears, which also contain some orange areas with higher distance. As a conclusion

the 3dMD model gives a very good result for the areas that are in focus, with some minor errors where the surface is rougher.

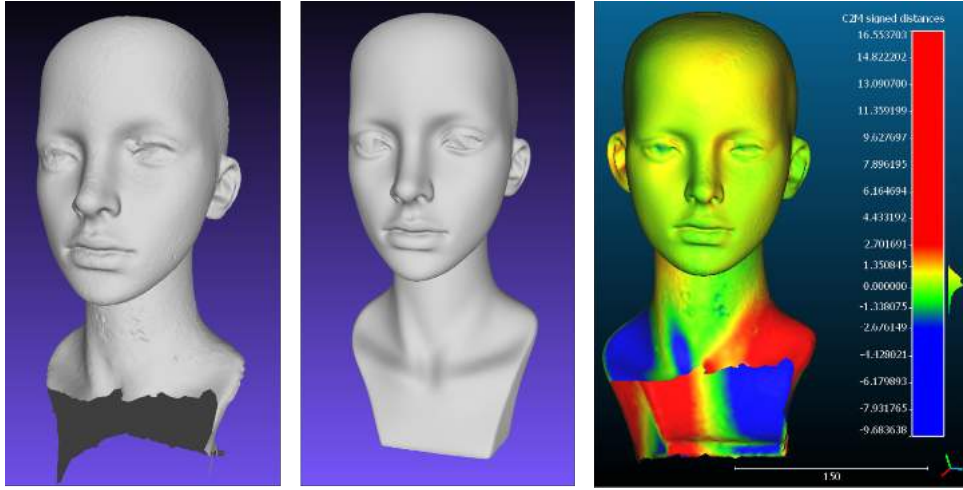


**Figure 4.13:** From left to right: the mesh from the 3dMD camera, the mesh from the HS3D scanner and the comparison between them.

The 3dMD model gives a better result than the models obtained using the imaged based method with a digital camera. As seen in figure 4.14, the 3dMD ranges between -1.3 to 1.3 mm in distance, compared to the camera model, Version 1, which ranges between -1.5 and 2 mm. Meaning that we have an improvement for the 3dMD model, but this difference is quite small considering the face.

By instead subjectively analyzing the details around the mouth and the nose, we notice that Version 1 has been smoothed and is not as accurate as the 3dMD model. This indicates that by smoothing the model the similarity to the real object increases overall, but this is at a cost of decreasing the details in the model.

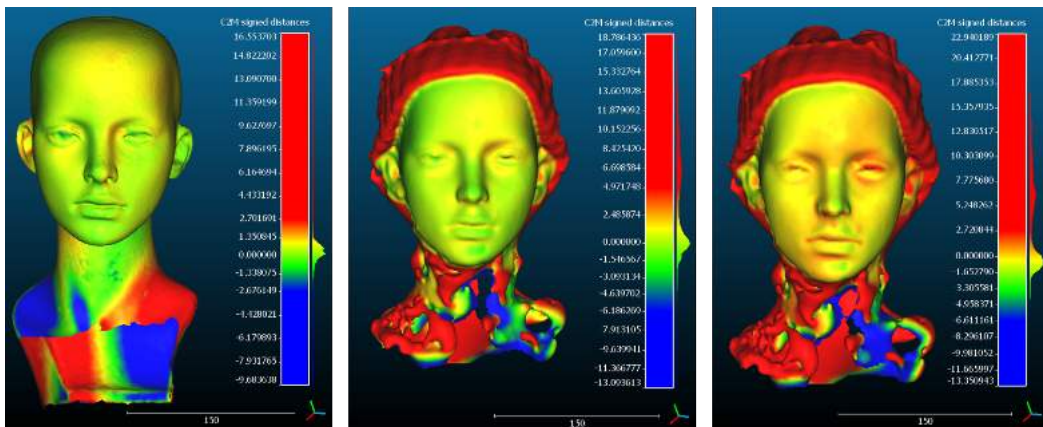


**Figure 4.14:** Comparing the 3dMD method and the digital camera to the HS3D. From left to right: the 3dMD mesh, the smoothed Version 1 and Version 1 with a lower reconstruction depth.

If we consider the aim of creating a patient specific bandage, the details might be

important depending on which area one wants to bandage. If the area is around the nose, or the mouth, you might not want to lose too much details. However, if the aim is to have a bandage around the chin, it could be more beneficial to smooth over the noise and the rough details. Therefore, it could also be beneficial to smooth the 3dMD model to reduce the rough surface.

### 4.2 3D Printing

The next step was to see how well the face of the mannequin could be printed. The obtained model from HS3D was used to try and print a concave mask of the face. Figure 4.15 shows the CAD model of the solid face and the belonging mask. The CAD model is then sliced in a slicer program, where the layer height and support structure is added, see figure 4.16.

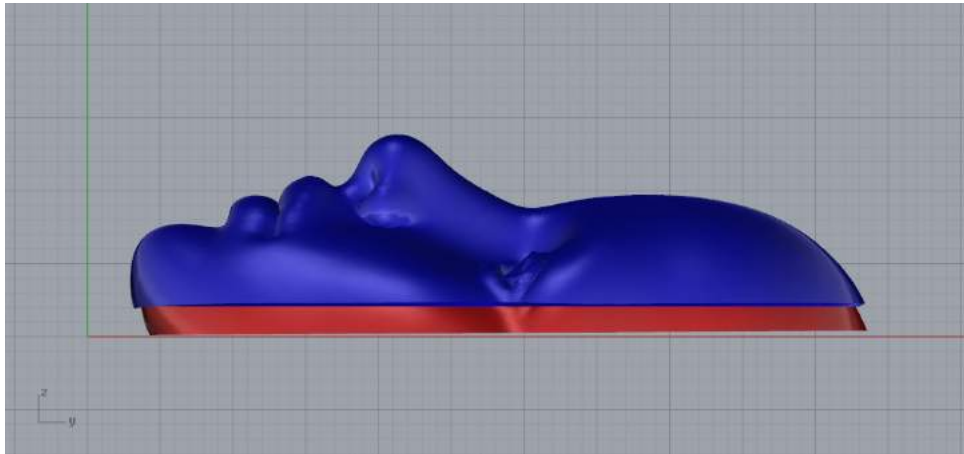


**Figure 4.15:** CAD model of the face mask in blue, and the solid face in red.

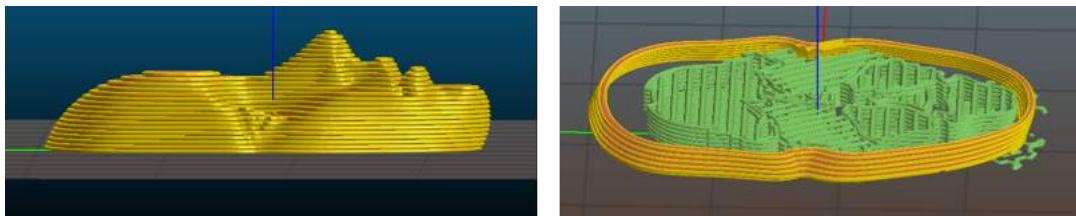


**Figure 4.16:** The sliced mask from the CAD model, with yellow indicating the layers and the green is the support structure.

The face mask was then printed in plastic and can be seen in figure 4.17. Here the hollow mask was printed with and without support structure. The result with the support structure is better than without support. Without the support the mask collapses where the angle is too high and the thickness too low.





**Figure 4.17:** Three models printed with PLA. From left to right: the solid face, the face mask without support and the face mask with support.

For a patient specific bandage, it is necessary to have a material that is more compatible with the skin. In figure 4.18 the solid face was printed with 3% CNF. Comparing this printed model to the sliced model in figure 4.16, we can see the slightly transparent layers of CNF. Since CNF is viscous, problems arise for finer structure such as the mouth and nose. For these areas we need a higher resolution than for other parts, meaning that we need to have a smaller diameter with lower layer height to get a higher resolution.

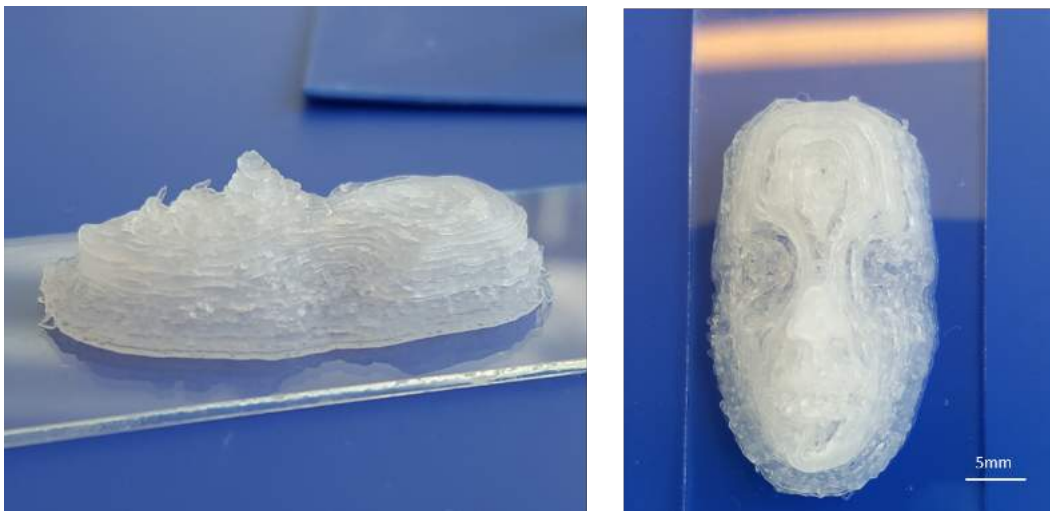


**Figure 4.18:** The solid face printed with 3% CNF at 110 Pa.

The next step is to print the face mask in CNF, which also requires a support structure. The support structure is printed with Nivea cream, and can be seen printed as a white filling in figure 4.19. The result of the printed CNF face mask with a support structure in Nivea can be seen in figure 4.20. Here we see that the resolution around the mouth and nose is lower than for the solid face in figure 4.18.

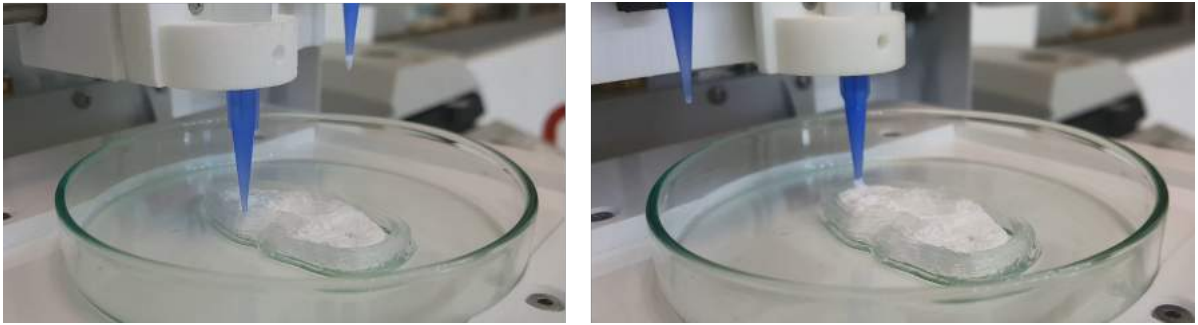


**Figure 4.19:** Image during the printing of the face mask. To the left is 3% CNF printed at 110 Pa and to the right is Nivea cream printed at 55 Pa.

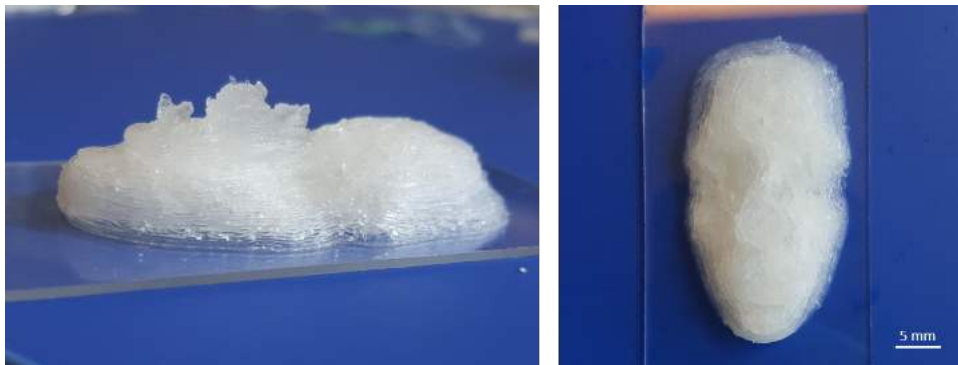


**Figure 4.20:** The face mask printed with 3% CNF at 110 Pa with a support structure printed with Nivea cream at 55 Pa.

When printing with two materials it is important to get the appropriate layer height for both materials, where it is especially important to get the same layer height. If the materials have different layer heights than the layer heights chosen in the Slicer software, a shift is created in the vertical direction during printing. This shift can cause the material to start printing lower than the actual layer, thus smearing the pattern that already has been printed. If the shift instead causes it to print higher than the actual layer, the result is that the material do not attach correctly to the previously layer.

In order to get an appropriate layer height of the materials, a printability analysis was done. From this analysis we can decide which resolution we want of the printed object, and from this set the correct printing speed. In figure 4.21, a printability analysis has been done for 4% CNF and Nivea cream. Here we see how the printing speed affects the diameter, where a higher speed gives a lower diameter. Since the layer height corresponds to the radius, an increasing the printing speed will give a higher resolution.

When then printing with two materials, it is important that they have similar layer height. By then choosing one diameter, we can from the graph chose the right printing speed for both materials. For example, if we want a layer height of 0.4mm,

the corresponding printing speed would be approximately 24mm/s for the CNF and 2mm/s for the Nivea.

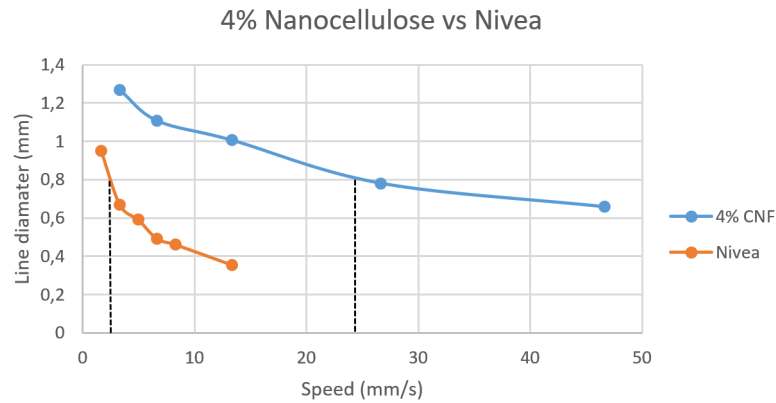


**Figure 4.21:** The printability analysis for 4% CNF versus the Nivea Cream, visualized as printing speed against the radius.

Since CNF mainly consists of water, it evaporates when dried in air. Therefore the masks were treated after the printing with different procedures. In figure 4.22, the result of the different procedures can be seen, where the masks have either been put in a calcium chloride bath to maintain its gel form, or freeze dried on a structure.



**Figure 4.22:** From left to right: the face mask printed with 1%, 3% and 4% CNF on a Nivea support. The masks were treated with a calcium chloride bath, freeze dried on the Nivea and freeze dried on a plastic support respectively.

Depending on what kind of bandage is needed, wet or dried, the printed CNF can be treated differently afterwards. If a wet bandage is needed some problem arises. The mask in the calcium chloride bath maintains its structure really well, but when removed from the bath it will eventually dry and lose its form. However, if a dry structure is wanted, it is suggested to freeze dry it on the printed support structure. This will maintain the structure rather well, but it is hard to prevent it from collapsing at all, see figure 4.23.



**Figure 4.23:** The face mask directly after printing and the freeze dried structure without Nivea cream.



# 5

## Discussion

The image based method using a digital camera gave good surfaces of the face with the right processing, even sufficient for 3D printing a patient specific dressing in certain conditions. The right process considers taking good resolution images of the object under controlled condition with even light and a unique background. If the image then contains noise it needs to be post processed, here the steps depend on the end use of the model.

If the aim is to create a model close to the real model and with an even surface, the processing procedure should be the following: sampling the point cloud, reconstructing the surface using default parameters, and then if needed, smoothing. This will most likely give a smooth model, relatively close to the ground truth.

However, one great drawback of using a digital camera is of course that it is not realistic to let a patient sit so still during the capturing of the images. For this purpose it would be beneficial to use several cameras, which will have the same settings. Using several cameras can allow you to take several photos from several angles at the same time. This setup will mimic the setup used by the 3dMD, which is a technique that handles movement of the patient very well.

Another disadvantage is also that the model is not according to the scale of the real object. Since the images can not tell the size of objects, the scale of the model will be arbitrary. However, by adding a measure in the images, the model can easily be scaled up close to the correct scale.

The HS3D method, or similar scanners, is the best option for creating a model with high accuracy. However, they are not good at imaging models that moves and it is not recommended to direct the lasers towards the eyes. The HS3D is designed for reverse engineering in industrial purposes, and not for medical purposes where moving objects like humans are involved. In the case of modelling a patient the 3dMD camera is nevertheless the best option. This method gives a high accuracy and is simple to use on patient, and even children who moves.

More problems instead occur when actually 3D printing the object. For harder materials, such as plastic (PLA), the convex surface is maintained very well if it has a supportive structure. When instead printing with fluid, viscous materials (CNF), it becomes harder to maintain the convex structure and prevent it from collapsing. Here it seems important to choose the right parameter in the G-code in order to get

the right layer height of the material. In this project the printed mask in nanocellulose was printed in a rather small scale. One solution to get a correct layer height of the material might be to scale it to a suitable size, or chose the material according to the scale. However, depending on how accurate the model needs to be, it is still possible to create a convex surface that maintains its shape overall both in a wet and a dry state.

The printability analysis is a way of getting an understanding of how the material behaves. By knowing how the material behaves it will become easier to maintain the printed convex structure. In this project, the calculated printing speed from the printability analysis was not tested due to time limit. The expected result would be a printed model with a higher resolution around the nose and the mouth. This printability analysis assumes a half circle of the printed line. A more correct procedure would be to firstly investigate the shape of the line and do calculations according to this shape. Another solution would be to measure the exact radius of the line, but this procedure is more time consuming the long run.

The next step in the project is to also measure how well the printed model mimics the CAD model. This could either be done by doing physical measurements or 3D scanning the printed model again for comparison. Then it would also be interesting to try and print the mask in different scales and with the parameters from the printability analysis.

# 6

## Conclusion

As a conclusion the image based method using a digital camera can, under the right conditions, be a sufficient method for 3D modelling smooth, convex surfaces. However, it needs further development to be used for 3D printing patient specific dressings. Instead, the advanced 3D camera method is a good, but expensive, option that gives really accurate 3D surfaces and is simple to use on moving patients. However, the problem arises when trying to maintain this accuracy when 3D printing a convex surface. The convex surface is dependent on choosing appropriate parameters according to the material to get a good resolution, and a supportive structure is needed to prevent it from collapsing.

This project has shown that a patient specific dressing may be a possibility in the future. The ideal scenario is that it will be possible to 3D scan a patient and then directly 3D print a bandage, which will be designed to fulfill the entire need of the wound of the patient.



# Bibliography

- [1] WHO. (Sep. 2016). Burns. World Health Organization, [Online]. Available: <http://www.who.int/mediacentre/factsheets/fs365/en/> (visited on 02/02/2017).
- [2] P. Appelgren, V. Björnhagen, K. Bragderyd, C. Jonsson, and U. Ransjö, “A prospective study of infections in burn patients”, *Burns : journal of the International Society for Burn Injuries*, vol. 28, no. 1, pp. 39–46, 2002. PMID: 11834328.
- [3] A. Heitland, A. Piatkowski, E. Noah, and N. Pallua, “Update on the use of collagen/glycosaminoglycate skin substitute-six years of experiences with artificial skin in 15 german burn centers”, *Burns : journal of the International Society for Burn Injuries*, vol. 30, no. 5, pp. 471–5, 2004. DOI: 10.1016/j.burns.2004.01.010.
- [4] C. Schubert and M. C. van Langeveld, “Innovations in 3D printing: A 3D overview from optics to organs”, *The British journal of ophthalmology*, vol. 98, no. 2, pp. 159–611, Nov. 2014. DOI: 10.1136/bjophthalmol-2013-304446.
- [5] C. Hull, “Apparatus for production of three-dimensional objects by stereolithography”, Patent US 4575330, 1984. [Online]. Available: <https://www.google.com/patents/us4575330>.
- [6] L. Mertz, “New world of 3-D printing offers ‘completely new ways of thinking’: Q&A with author, engineer, and 3-d printing expert hod lipson”, *IEEE Pulse*, vol. 4, no. 6, pp. 12–14, Nov. 2013. DOI: 10.1109/MPUL.2013.2279615.
- [7] A. Atala and J. J. Yoo, *Essential of 3D biofabrication and translation*. United States, Massachusetts: Academic Press, 2015.
- [8] F. Remondino and S. El-Hakim, “Image-based 3D modelling: A review”, vol. 21, no. 115, pp. 269–291, Aug. 2006. DOI: 10.1111/j.1477-9730.2006.00383.x.
- [9] V. Evgenikou and A. Georgopoulos, “Investigating 3D reconstruction methods for small artifacts”, *ISPRS - International Archives of the Photogrammetry, Remote Sensing and Spatial Information Sciences*, vol. XL-5/W4, pp. 101–108, Feb. 2015. DOI: 10.5194/isprsarchives-XL-5-W4-101-2015.
- [10] S. S. Scherer-Pietramaggiori, G. Pietramaggiori, and D. P. Orgill, “Skin graft”, in *Plastic Surgery: Volume 3: Craniofacial, Head and Neck Surgery Pediatric Plastic Surgery (Expert Consult - Online)*, Saunders, 2012, ch. 17, ISBN: 9781455710546.
- [11] R. E. Billingham and P. B. Medawar, “Contracture and intussusceptive growth in the healing of extensive wounds in mammalian skin”, *J. Anat.*, vol. 89, no. Pt 1, pp. 114–123, Jan. 1955, Department of Zoology, University College,

- University of London. [Online]. Available: <https://www.ncbi.nlm.nih.gov/pmc/articles/PMC1244731/#reference-sec>.
- [12] K. Petkar, P. Dhanraj, and H. Sreekar, "Vacuum closure as a skin-graft dressing: A comparison against conventional dressing", *European Journal of Plastic Surgery*, vol. 35, no. 8, pp. 579–584, Apr. 2012. DOI: 10.1007/s00238-012-0698-y.
  - [13] M. L. Venturi, C. E. Attinger, A. N. Mesbahi, C. L. Hess, and K. S. Graw, "Mechanisms and clinical applications of the vacuum-assisted closure (VAC) device", *American Journal of Clinical Dermatology*, vol. 6, no. 3, pp. 185–194, 2005. DOI: 10.2165/00128071-200506030-00005.
  - [14] C. Xia, A. Yu, B. Qi, M. Zhou, Z. Li, and W. Wang, "Analysis of blood flow and local expression of angiogenesis-associated growth factors in infected wounds treated with negative pressure wound therapy", *Molecular Medicine Reports*, Feb. 2014. DOI: 10.3892/mmr.2014.1997.
  - [15] W. J, S. P, S. M, and C. WP, "Negative pressure wound therapy for skin grafts and surgical wounds healing by primary intention", *Cochrane Wounds Group*, vol. 10, no. CD009261, 2014. DOI: 10.1002/14651858.CD009261.pub3..
  - [16] J. Sturm, E. Bylow, F. Kahl, and D. Cremers, "CopyMe3D: Scanning and printing persons in 3D", in *Lecture Notes in Computer Science*, Springer Nature, 2013, pp. 405–414. DOI: 10.1007/978-3-642-40602-7\_43.
  - [17] Y. Furukawa and C. Hernández, "Multi-view stereo: A tutorial", *Foundations and Trends in Computer Graphics and Vision*, vol. 9, no. 1-2, pp. 1–148, 2015. DOI: 10.1561/06000000052.
  - [18] D. A. Tingdahl, "Image based 3D reconstruction and its application", PhD thesis, Katholieke Universiteit Leuven, Heverlee, Belgium, 2013.
  - [19] M. Wilczkowiak, *3D modeling from images using geometric constraints*. Institut National Polytechnique de Grenoble - INPG, Apr. 2004.
  - [20] S. Haner, "View planning and refractive modeling for structure and motion", PhD thesis, Lund University, 2015.
  - [21] M. Yirci, "A comparative study on polygon mesh simplification algorithms", Master's thesis, Middle East Technical University, Sep. 2009.
  - [22] M. Franc, "Methods for polygonal mesh simplification", PhD thesis, University of West Bohemia, 2002.
  - [23] M. B. Michael Kazhdan and H. Hoppe, "Poisson surface reconstruction", *The Eurographics Association 2006*, pp. 61–70, Jun. 2006.
  - [24] M. Kazhdan and H. Hoppe, "Screened poisson surface reconstruction", *ACM Transactions on Graphics (TOG)*, vol. 32, no. 3, p. 29, 2013.
  - [25] M. Corsini, P. Cignoni, and R. Scopigno, "Efficient and flexible sampling with blue noise properties of triangular meshes", *IEEE Transaction on Visualization and Computer Graphics*, vol. 18, no. 6, pp. 914–924, 2012. DOI: 10.1109/TVCG.2012.34. [Online]. Available: <http://vcg.isti.cnr.it/Publications/2012/CCS12>.
  - [26] J. Vollmer, R. Mencl, and H. Muller, "Improved laplacian smoothing of noisy surface meshes", *Computer Graphics Forum*, vol. 18, no. 3, pp. 131–138, Sep. 1999. DOI: 10.1111/1467-8659.00334. [Online]. Available: <https://doi.org/10.1111/1467-8659.00334>.

- [27] P. S. Heckbert and M. Garland, “Optimal triangulation and quadric-based surface simplification”, *Computational Geometry*, vol. 14, no. 1-3, pp. 49–65, Nov. 1999. DOI: 10.1016/s0925-7721(99)00030-9.
- [28] C. S. Simon Boyé Gael Guennebaud, “Least squares subdivision surfaces”, *Computer Graphics Forum (Proceedings of Pacific Graphics 2010)*, vol. 7, no. 29, 2010. [Online]. Available: <https://hal.inria.fr/inria-00524555>.
- [29] P. Cignoni, C. Rocchini, and R. Scopigno, “Metro: Measuring error on simplified surfaces”, in *Computer Graphics Forum*, Blackwell Publishers, vol. 17, 1998, pp. 167–174.
- [30] I. Gibson, D. Rosen, and B. Stucker, *Additive manufacturing technologies*. Springer New York, 2015. DOI: 10.1007/978-1-4939-2113-3. [Online]. Available: <https://doi.org/10.1007/978-1-4939-2113-3>.
- [31] A. Bandyopadhyay, T. Gualtieri, and S. Bose, “Global engineering and additive manufacturing”, in *Additive Manufacturing*, CRC Press, Aug. 2015, pp. 1–18. DOI: 10.1201/b18893-2. [Online]. Available: <https://doi.org/10.1201/b18893-2>.
- [32] M. Kumar and B. Morrison, “Personalized implants and additive manufacturing”, in *Additive Manufacturing*, CRC Press, Aug. 2015, pp. 351–366. DOI: 10.1201/b18893-14. [Online]. Available: <https://doi.org/10.1201/b18893-14>.
- [33] “Rapid prototyping & manufacturing— fundamentals of stereolithography”, *Journal of Manufacturing Systems*, vol. 12, no. 5, pp. 430–433, 1993. DOI: 10.1016/0278-6125(93)90311-g. [Online]. Available: [https://doi.org/10.1016/0278-6125\(93\)90311-g](https://doi.org/10.1016/0278-6125(93)90311-g).
- [34] “Selective laser sintering, birth of an industry”, 2012, accessed on May 23, 2017. [Online]. Available: <http://www.me.utexas.edu/news/news/selective-laser-sintering-birth-of-an-industry>.
- [35] R. Vaidyanathan, “Additive manufacturing technologies for polymers and composites”, in *Additive Manufacturing*, CRC Press, Aug. 2015, pp. 19–64. DOI: 10.1201/b18893-3. [Online]. Available: <https://doi.org/10.1201/b18893-3>.
- [36] S. V. Murphy and A. Atala, “3D bioprinting of tissues and organs”, *Nature Biotechnology*, vol. 32, no. 8, pp. 773–785, Aug. 2014. DOI: 10.1038/nbt.2958. [Online]. Available: <https://doi.org/10.1038/nbt.2958>.
- [37] M. Nakamura, S. Iwanaga, C. Henmi, K. Arai, and Y. Nishiyama, “Biomatrices and biomaterials for future developments of bioprinting and biofabrication”, *Biofabrication*, vol. 2, no. 1, p. 014110, Mar. 2010. DOI: 10.1088/1758-5082/2/1/014110. [Online]. Available: <https://doi.org/10.1088/1758-5082/2/1/014110>.
- [38] A. Skardal, “Bioprinting essentials of cell and protein viability”, in *Essentials of 3D Biofabrication and Translation*, Elsevier, 2015, pp. 1–17. DOI: 10.1016/b978-0-12-800972-7.00001-3. [Online]. Available: <https://doi.org/10.1016/b978-0-12-800972-7.00001-3>.
- [39] N. E. Fedorovich, J. Alblas, J. R. de Wijn, W. E. Hennink, A. J. Verbout, and W. J. Dhert, “Hydrogels as extracellular matrices for skeletal tissue engineering: State-of-the-art and novel application in organ printing”, *Tissue Engineer-*

- ing*, vol. 13, no. 8, pp. 1905–1925, Aug. 2007. DOI: 10.1089/ten.2006.0175. [Online]. Available: <https://doi.org/10.1089/ten.2006.0175>.
- [40] S. Iwanaga, K. Arai, and M. Nakamura, “Inkjet bioprinting”, in *Essentials of 3D Biofabrication and Translation*, Elsevier, 2015, pp. 61–79. DOI: 10.1016/b978-0-12-800972-7.00004-9. [Online]. Available: <https://doi.org/10.1016/b978-0-12-800972-7.00004-9>.
- [41] *Static-3dmd systems*. [Online]. Available: <http://www.3dmd.com/3dmd-systems/> (visited on 05/24/2017).
- [42] *Portable 3D scanners: Handyscan 3D portable 3D scanners: Handyscan 3D*. [Online]. Available: <https://www.creaform3d.com/en/metrology-solutions/portable-3d-scanner-handyscan-3d> (visited on 05/24/2017).
- [43] *Visualsfm : A visual structure from motion system*, 2011. [Online]. Available: <http://ccwu.me/vsfm/> (visited on 05/24/2017).
- [44] C. Wu, S. Agarwal, B. Curless, and S. M. Seitz, “Multicore bundle adjustment”, in *CVPR 2011*, IEEE, Jun. 2011. DOI: 10.1109/cvpr.2011.5995552. [Online]. Available: <https://doi.org/10.1109/cvpr.2011.5995552>.
- [45] Y. Furukawa and J. Ponce, “Accurate, dense, and robust multi-view stereopsis”, in *2007 IEEE Conference on Computer Vision and Pattern Recognition*, IEEE, Jun. 2007. DOI: 10.1109/cvpr.2007.383246. [Online]. Available: <https://doi.org/10.1109/cvpr.2007.383246>.
- [46] P. Cignoni, M. Callieri, M. Corsini, M. Dellepiane, F. Ganovelli, and G. Ranzuglia, “Meshlab: An open-source mesh processing tool”, in *Eurographics Italian Chapter Conference*, V. Scarano, R. D. Chiara, and U. Erra, Eds., The Eurographics Association, 2008, ISBN: 978-3-905673-68-5. DOI: 10.2312/LocalChapterEvents/ItalChap/ItalianChapConf2008/129–136.



# Acronyms

**CAD** Computer-Aided Design. 6, 9, 16, 23, 36, 42

**CNF** Cellulose Nanofibrils. 23, 24, 37–39, 41

**CT** Computerized Tomography. 2, 16

**DoG** Difference-of-Gaussian. 7

**FDM** Fused Deposition Modeling. 17

**HS3D** HandyScan 3D. 20, 21, 23, 27, 29–34, 36, 41

**ICP** Iterative Closest Point. 23

**LOD** Levels of Detail. 13, 15

**LS3** Least Squares Subdivision Surfaces. 14

**MRI** Magnetic Resonance Imaging. 2, 16

**MVS** Multi-View Stereo. 8, 20, 22, 27, 34

**NURB** Non-Uniform Rational B-Splines. 9

**OBJ** Object. 16

**PLA** Polylactide. 23, 37, 41

**PLY** Polygon File Format. 16

**PMVS** Patch-based Multi-View Stereo. 22

**RANSAC** Random Sample Consensus. 7

**SfM** Structure from Motion. 7–9, 27, 34

**SIFT** Scale-Invariant Feature Transform. 7

**SLA** Stereolithography. 17

**SLS** Selective Laser Sintering. 17

**STL** Stereolithography. 16, 17

**VAC** Vacuum-Assisted Closure. 5